Cell Reports

Article

Type I Interferon Receptor Signaling in Astrocytes Regulates Hippocampal Synaptic Plasticity and Cognitive Function of the Healthy CNS

Graphical Abstract

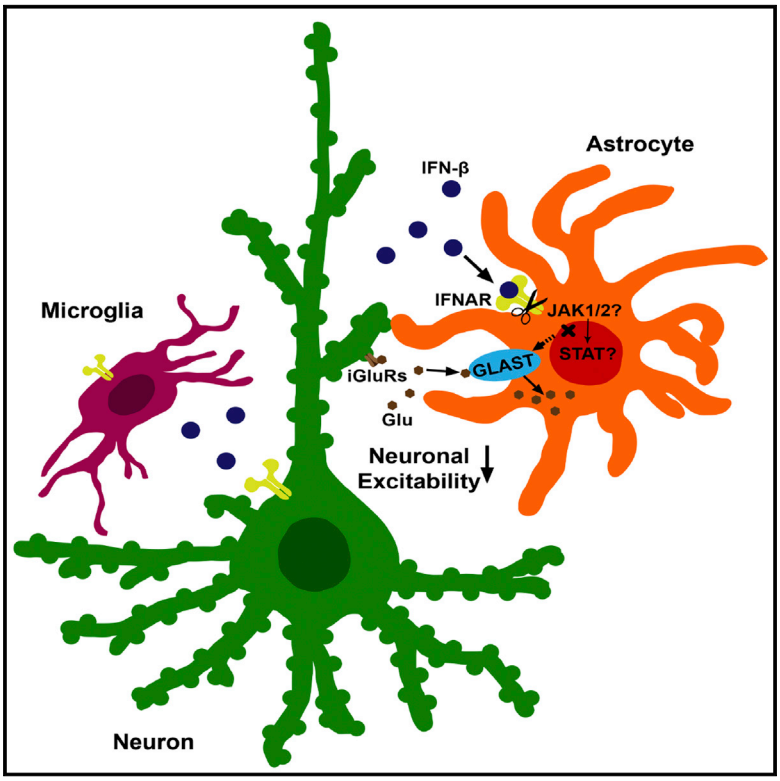

Highlights

- Baseline levels of IFNAR signaling are critical for synaptic plasticity
- IFNAR signaling is needed acutely during synaptic plasticity
- Astrocyte IFNAR signaling may regulate synaptic plasticity by GLAST modulation

Authors

Shirin Hosseini,
Kristin Michaelsen-Preusse,
Gayane Grigoryan, Chintan Chhatbar,
Ulrich Kalinke, Martin Korte

Correspondence

m.korte@tu-bs.de

In Brief

Interferon (IFN) signaling within the CNS is critical for synaptic plasticity and processes of learning and memory formation under physiological conditions. Hosseini et al. provide evidence that the type I IFN receptor (IFNAR) is mediating this effect via the glutamate-aspartate transporter (GLAST) in astrocytes by regulating synaptic glutamate levels.

Hosseini et al., 2020, Cell Reports *31*, 107666
May 19, 2020
https://doi.org/10.1016/j.celrep.2020.107666

CellPress

Cell Reports

CellPress
OPEN ACCESS

Article

Type I Interferon Receptor Signaling in Astrocytes Regulates Hippocampal Synaptic Plasticity and Cognitive Function of the Healthy CNS

Shirin Hosseini,[1,2] Kristin Michaelsen-Preusse,[1] Gayane Grigoryan,[3] Chintan Chhatbar,[4,5] Ulrich Kalinke,[4] and Martin Korte[1,2,6,*]

[1]Department of Cellular Neurobiology, Zoological Institute, TU Braunschweig, 38106 Braunschweig, Germany
[2]Helmholtz Centre for Infection Research, Neuroinflammation and Neurodegeneration Group, 38124 Braunschweig, Germany
[3]Department of Systemic and Cellular Neurophysiology, Institute for Physiology I, Faculty of Medicine, University of Freiburg, 79104 Freiburg, Germany
[4]Institute for Experimental Infection Research, TWINCORE, Centre for Experimental and Clinical Infection Research, a joint venture between the Helmholtz Centre for Infection Research, Braunschweig, and the Hannover Medical School, 30625 Hannover, Germany
[5]Present address: Institute of Neuropathology, Faculty of Medicine, University of Freiburg, 79106 Freiburg, Germany
[6]Lead Contact
*Correspondence: m.korte@tu-bs.de
https://doi.org/10.1016/j.celrep.2020.107666

SUMMARY

Type I interferon receptor (IFNAR) signaling is a hallmark of viral control and host protection. Here, we show that, in the hippocampus of healthy IFNAR-deficient mice, synapse number and synaptic plasticity, as well as spatial learning, are impaired. This is also the case for IFN-β-deficient animals. Moreover, antibody-mediated IFNAR blocking acutely interferes with neuronal plasticity, whereas a low-dose application of IFN-β has a positive effect on dendritic spine structure. Interfering with IFNAR signaling in different cell types shows a role for cognitive function and synaptic plasticity specifically mediated by astrocytes. Intriguingly, levels of the astrocytic glutamate-aspartate transporter (GLAST) are reduced significantly upon IFN-β treatment and increase following inhibition of IFNAR signaling. These results indicate that, besides the prominent role for host defense, IFNAR is important for synaptic plasticity as well as cognitive function. Astrocytes are at the center stage of this so-far-unknown signaling cascade.

INTRODUCTION

Type I interferons (IFNs) are crucial for viral control early after infection (Fensterl et al., 2015; Müller et al., 1994). However, they can induce dose-dependent neuronal damage and behavioral disturbances in both humans and animals (Crow and Manel, 2015; Wilson et al., 2002). In mammals, IFN-α and IFN-β are the most important type I IFN members, which bind to the common type I IFN receptor (IFNAR) (Fensterl et al., 2015). Genetically modified mice lacking the IFNAR1 subunit are devoid of a functional IFN system and show enhanced susceptibility upon infection with viruses (Müller et al., 1994). Interestingly, the roles of IFN-α and IFN-β are not only limited to antiviral and immunomodulatory actions, but both IFNs can also regulate homeostatic processes in the periphery and the CNS (Blank and Prinz, 2017). Under physiological conditions, low levels are thought to maintain expression of STAT1 (Goldmann et al., 2016). Since STAT1 activates the transcription of a number of IFN-stimulated genes, it is believed that this allows cells to enhance IFN-α/β production rapidly as necessary via auto-amplification (Gough et al., 2010; Tovey et al., 1987). Relatively low baseline levels were also detected in the CNS by ELISA (Goldmann et al., 2016; Hwang et al., 1995), and it is clear that all cell types of the CNS can produce and respond to IFN. Therefore, the question arises of whether these low levels of IFN might fulfill an additional purpose beyond rendering the CNS ready to fight potential viral infection. Evidence indeed suggests that IFN can promote the development of cortical, hippocampal, and cholinergic neurons (Vikman et al., 2001). IFN-β-deficient mice (*Ifnb*$^{-/-}$) show increased neuronal apoptosis and reduced neurite network formation (Ejlerskov et al., 2015), suggesting that in healthy conditions, baseline levels of constant IFN secretion in the CNS contribute to neuronal survival, branching, and neurite outgrowth. Furthermore, low-level IFN-β treatment (500–5000 U/ml) was sufficient to protect neurons *in vitro* against HIV-1 envelope glycoprotein 120-induced neurotoxicity without any changes in neuronal survival (Thaney et al., 2017). In addition to the role of IFN for neuronal development and survival, experiments have indicated important roles of IFN for synaptic transmission and function (Ignatowski and Spengler, 2008). Neurons express IFNAR on both pre- and postsynaptic membranes (Vikman et al., 1998), and IFNs have indeed been shown to modulate neuronal excitability (Prieto-Gomez et al., 1983). On the other hand, it was shown that high concentrations of IFN-α in rat hippocampal acute slices led to a reduction in short-term potentiation and impaired long-term potentiation (LTP) (D'Arcangelo et al., 1991;

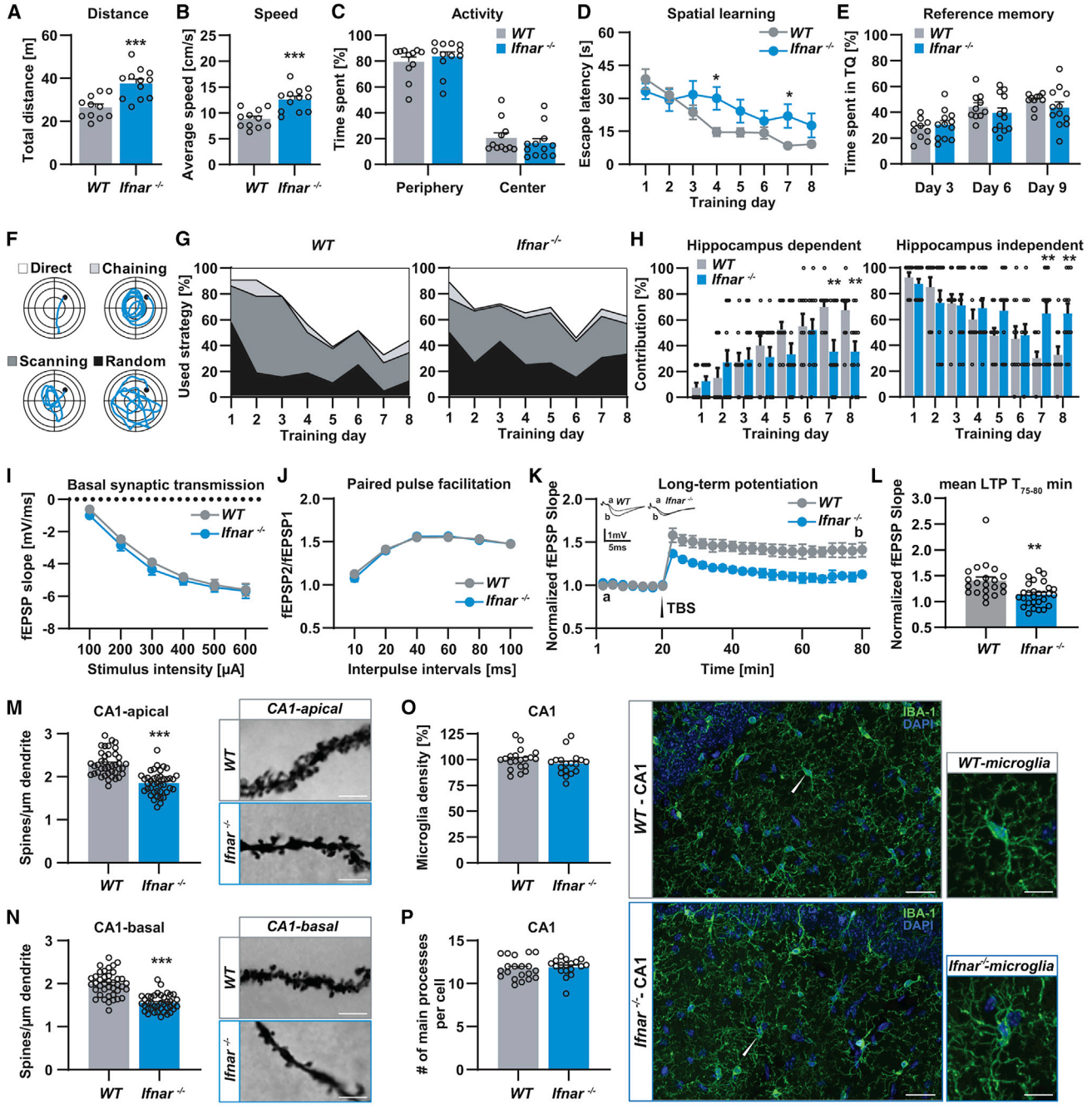

Figure 1. Impaired Cognitive Function and Synaptic Plasticity in *Ifnar*$^{-/-}$ Animals

(A and B) *Ifnar*$^{-/-}$ mice exhibited (A) a longer distance traveled with (B) higher average speed compared to *WT* mice.

(C) Time of both tested groups spent in the periphery versus the center part of the open-field arena did not differ between genotypes (n of mice in *WT* = 11, *Ifnar*$^{-/-}$ n = 12).

(D) *Ifnar*$^{-/-}$ mice showed a higher escape latency and, therefore, impaired spatial learning compared to *WT* animals.

(E) Percentage of time spent in the target quadrant (TQ) did not differ significantly between both tested groups during reference memory tests.

(F) Example tracks of searching strategies used during the Morris water maze training.

(G) A reduction in the use of the hippocampus-dependent strategy by *Ifnar*$^{-/-}$ mice became apparent.

(H) Searching strategy quantification revealed that the hippocampus-dependent strategy was significantly decreased and hippocampus-independent strategies were increased in *Ifnar*$^{-/-}$ mice compared to *WT* (n of mice in *WT* = 10, *Ifnar*$^{-/-}$ n = 12).

(I) Input-output curves showed no difference in basal synaptic transmission between *WT* and *Ifnar*$^{-/-}$ mice.

(legend continued on next page)

Mendoza-Fernández et al., 2000). IFN signaling may therefore act as a double-edged sword, which could be either detrimental or neuroprotective, depending on the dose. However, the detailed neurophysiological mechanisms involved in IFN signaling, especially in the absence of infection, and its importance for cognitive function, such as memory formation, remain elusive. Using either conventional or cell-type-specific IFNAR knockout mice as well as a low-dose IFN-β application, we provide evidence that IFNAR signaling in astrocytes is involved in synaptic plasticity and memory formation, possibly by modulating glutamate-aspartate transporter (GLAST) expression.

RESULTS

IFNAR Signaling Regulates Hippocampal Function

In order to study the physiological role of IFNAR signaling in the CNS for hippocampal function and synaptic plasticity, first, conventional IFNAR-deficient mice (*Ifnar*$^{-/-}$) were used (Figure 1). To investigate general locomotor activity and to initially screen for anxiety-related behavior, wild-type (*WT*) and *Ifnar*$^{-/-}$ mice were tested for 5 min in the open-field arena (Figures 1A–1C). *Ifnar*$^{-/-}$ mice traveled a significantly longer distance, with higher average speed, compared to *WT* mice (distance, *WT*: 26.47 ± 1.59 m, *Ifnar*$^{-/-}$: 37.61 ± 2.03 m, unpaired t test: t = 4.25, df = 21, p = 0.0004; Figure 1A; speed, *WT*: 8.82 ± 0.53 cm/s, *Ifnar*$^{-/-}$: 12.57 ± 0.66 cm/s, unpaired t test: t = 4.34, df = 21, p = 0.0003; Figure 1B). However, *WT* and *Ifnar*$^{-/-}$ mice spent comparable times in the periphery and center zones of the open field (periphery, *WT*: 79.45% ± 3.80%, *Ifnar*$^{-/-}$: 83.59% ± 3.55%; center, *WT*: 20.54% ± 3.80%, *Ifnar*$^{-/-}$: 16.40% ± 3.55%; unpaired t test: t = 0.79, df = 21, p = 0.43; Figure 1C). The results of this test, therefore, revealed hyperactivity in *Ifnar*$^{-/-}$ mice, but no significant alterations in anxiety-related behavior. As a next step to identify the putative role of IFNAR signaling for cognitive function, *Ifnar*$^{-/-}$ and *WT* mice were trained for 8 days in the Morris water maze. As shown in Figure 1D, the escape latency progressively decreased over 8 days of acquisition training in *WT* animals, but not in *Ifnar*$^{-/-}$ mice (one-way ANOVA: $F_{WT}(7, 72) = 16.29$, $p < 0.0001$ and $F_{Ifnar-/-}(7, 88) = 1.31$, $p = 0.25$). A day-by-day comparison of the data between both tested groups also showed that the escape latency on acquisition days 4 and 7 was significantly higher in *Ifnar*$^{-/-}$ animals compared to *WT* mice (two-way ANOVA: $F_{Treatment}(1, 160) = 9.17$, $p = 0.002$, Fisher's LSD test: day 4: p = 0.013, day 7: p = 0.03; Figure 1D). Both groups were submitted to reference memory tests (probe trials without the platform) on days 3 and 6 prior to the training session and 24 h after the last training session on day 9 (Figure 1E). On days 6 and 9, *Ifnar*$^{-/-}$ mice (day 6: 39.38% ± 4.11%; day 9: 43.57% ± 4.39%) spent slightly less time in the target quadrant (TQ) compared to *WT* animals (day 6: 44.20% ± 3.24%; day 9: 49.12% ± 1.82%), although this difference was not statistically significant (day 6, unpaired t test: t = 0.89, df = 20, p = 0.38; day 9, unpaired t test: t = 1.08, df = 20, p = 0.29; Figure 1E).

To further analyze differences in the quality of spatial memory formation, searching strategies were assessed (Figures 1F–1H). The results revealed that in both *WT* and *Ifnar*$^{-/-}$ mice, the use of hippocampus-dependent direct swimming increased over the training time. However, this progression was significantly decreased in *Ifnar*$^{-/-}$ mice compared to *WT* animals (day 7, *WT*: 70% ± 5% and *Ifnar*$^{-/-}$: 35.41% ± 8.95%; day 8, *WT*: 67.50% ± 6.50% and *Ifnar*$^{-/-}$: 35.42% ± 7.82%), whereas hippocampus-independent search strategies were significantly increased, especially on days 7 and 8 of the acquisition training in *Ifnar*$^{-/-}$ animals, compared to *WT* mice (day 7, *WT*: 30% ± 5% and *Ifnar*$^{-/-}$: 64.59% ± 8.95%; day 8: *WT*: 32.50% ± 6.50% and *Ifnar*$^{-/-}$: 64.58% ± 7.82%; Fisher's LSD, day 7: p = 0.003, day 8: p = 0.005; Figures 1G and 1H).

The findings of the Morris water maze test indicated a hippocampus-dependent learning deficit in *Ifnar*$^{-/-}$ mice. Therefore, as a next step, hippocampal synaptic plasticity was investigated to reveal potential cellular mechanisms responsible for this deficit. For this purpose, field excitatory postsynaptic potentials (fEPSPs) in the *stratum radiatum* of the hippocampal CA1 area in response to stimulation of the Schafer collaterals were recorded from hippocampal slices of 6–8-week-old animals (Figures 1I–1L). The input-output curve of the fEPSP slope dependence to the stimulation intensity did not reveal any significant difference between *Ifnar*$^{-/-}$ and *WT* mice (two-way ANOVA: $F(1, 282) = 2.64$, $p = 0.10$; Figure 1I). Thus, basal synaptic transmission was not affected by IFNAR signaling deficiency. Analysis of paired-pulse facilitation (PPF) of fEPSPs to afferent stimulation, a form of short-term synaptic plasticity, was not affected in the absence of IFNAR in hippocampal slices (two-way ANOVA: $F(1, 282) = 0.45$, $p = 0.49$; Figure 1J). Next, to study the role of IFNAR signaling in synaptic plasticity, LTP was analyzed. LTP was induced by theta-burst stimulation (TBS). Slices of *Ifnar*$^{-/-}$ mice showed a significantly impaired LTP compared to *WT* animals (two-way ANOVA: $F(1, 940) = 252.8$, $p < 0.0001$; Figure 1K). Also, the mean value of the maintenance phase of LTP (displayed as the last 5 min of the recording) was significantly diminished in *Ifnar*$^{-/-}$ mice (*WT*: 1.40 ± 0.07, *Ifnar*$^{-/-}$: 1.13 ± 0.04, unpaired t test: t = 3.37, df = 47, p = 0.001; Figure 1L). To investigate the potential cellular mechanism underlying the observed impairment in spatial learning and LTP in *Ifnar*$^{-/-}$ mice, hippocampal neuron morphology was studied

(J) No alteration was found in paired-pulse facilitation (PPF) between *WT* and *Ifnar*$^{-/-}$ mice.
(K) *Ifnar*$^{-/-}$ mice showed a significant impaired LTP induced by TBS.
(L) The mean LTP magnitude (T 75–80min) was significantly lower in *Ifnar*$^{-/-}$ animals than in *WT* mice (n of slices in *WT* = 21, *Ifnar*$^{-/-}$ n = 28).
(M and N) Spine density of (M) apical and (N) basal dendrites of CA1 pyramidal neurons was diminished in *Ifnar*$^{-/-}$ mice compared to *WT*. Representative images show dendritic spines of hippocampal CA1 neurons in both tested groups (scale bar, 2 μm; n of mice in each group = 4, n of dendrites in each group = 40).
(O) Microglia density and (P) number of primary processes as an indicator for the activation status in the CA1 hippocampal subregion of *Ifnar*$^{-/-}$ mice showed no obvious signs of inflammation. Representative examples show anti-IBA-1 immunostaining of the CA1 region in both tested groups (scale bar, 10 μm; n of animals in each group = 4, n of ROIs in *WT* = 20, *Ifnar*$^{-/-}$ = 18, n of randomly selected microglia in *WT* = 120, *Ifnar*$^{-/-}$ = 108).
Data are presented as mean ± SEM. *p < 0.05, **p < 0.01, ***p < 0.001, compared to *WT*.

(Figures 1M and 1N). Alterations in dendritic spine density and morphology have been shown to correlate with defects in synaptic plasticity and cognitive function in general (Moser et al., 1994). Dendritic spine counting on apical and basal dendrites (Figures 1M and 1N) of CA1 pyramidal neurons in the hippocampus of *Ifnar*$^{-/-}$ mice revealed a significant reduction (apical dendrite, Δ-19.44%, unpaired t test: t = 7.15, df = 78, p < 0.0001; basal dendrite, Δ-22.01%, unpaired t test: t = 8.19, df = 78, p < 0.0001).

Previously, it was shown that *Ifnar*$^{-/-}$ mice are more sensitive to infections, as they lack the first line of defense against viral pathogens (Müller et al., 1994; Wei et al., 2017). Therefore, to confirm that the observed impairments in cognitive function and synaptic plasticity were not due to neuroinflammation and microgliosis, which might affect synaptic plasticity (Chhatbar et al., 2018; Riazi et al., 2015), microglia density (Figure 1O) and possible activation status (Figure 1P) in the CA1 hippocampal subregion of *WT* and *Ifnar*$^{-/-}$ mice were assessed. Microglia density did not differ in *Ifnar*$^{-/-}$ mice compared to *WT* mice (unpaired t test: t = 1.19, df = 36, p = 0.24; Figure 1O). Earlier studies indicated that a reduced number of primary processes can reflect an elevated activation status of microglia (Papageorgiou et al., 2015; Wolf et al., 2017); however, no alterations in the number of main processes were found in *Ifnar*$^{-/-}$ compared to *WT* animals (unpaired t test: t = 0.47, df = 36, p = 0.63; Figure 1P). It therefore needs to be emphasized that IFNAR deficiency was not associated with a detectable elevation of neuroinflammation in the brain of healthy animals that would lead to reduced synaptic plasticity and memory.

IFNAR Signaling in Astrocytes Regulates Hippocampal Function

We showed that IFNAR signaling is crucial for hippocampal synapse function. However, the mechanisms, and especially the cell types involved, remain elusive. Therefore, cell-type-specific IFNAR deletion was used to determine the precise role of IFNAR signaling in cognitive processes under healthy conditions.

For this purpose, NesCre$^{+/-}$IFNAR$^{fl/fl}$ mice with a selective IFNAR deletion in neuroectodermal cells of the CNS including neurons, astrocytes, and oligodendrocytes, but not microglia (Chhatbar et al., 2018; Detje et al., 2015, 2009), as well as Syn1Cre$^{+/-}$IFNAR$^{fl/fl}$ mice with neuron-specific IFNAR deletion (Zhu et al., 2001) and GFAPCre$^{+/-}$IFNAR$^{fl/fl}$ mice with astrocyte-specific IFNAR deletion (Bajenaru et al., 2002), were investigated. In this study, mice with negative Cre expression obtained from mating between cell-specific promoter-driven Cre transgenic mice and IFNAR$^{fl/fl}$ animals were considered as littermate control (Ctrl) animals. Cre-negative mice in all three groups (NesCre$^{-/-}$IFNAR$^{fl/fl}$, Syn1Cre$^{-/-}$IFNAR$^{fl/fl}$, and GFAPCre$^{-/-}$IFNAR$^{fl/fl}$) exhibited similar characteristics without any significant differences. As a consequence, we chose NesCre$^{-/-}$IFNAR$^{fl/fl}$ mice (Nes-Cre-negative expression) as the Ctrl group (Figure S1).

First, all conditional knockout mice were examined in the open-field arena for 5 min (Figures 2A–2C). Analysis of the total distance traveled (Figure 2A), average speed (Figure 2B), and general activity in the periphery and center zones of the arena (Figure 2C) revealed no significant differences from the Ctrl group (distance, Ctrl: 21.88 ± 2.40 m, NesCre$^{+/-}$IFNAR$^{fl/fl}$: 27.10 ± 1.70 m, Syn1Cre$^{+/-}$IFNAR$^{fl/fl}$: 19.51 ± 2.12 m, GFAPCre$^{+/-}$IFNAR$^{fl/fl}$: 22.89 ± 1.64 m; one-way ANOVA: F(3, 42) = 2.82, p = 0.0504; Figure 2A; speed, Ctrl: 7.28 ± 0.80 cm/s, NesCre$^{+/-}$IFNAR$^{fl/fl}$: 9.03 ± 0.56 cm/s, Syn1Cre$^{+/-}$IFNAR$^{fl/fl}$: 6.50 ± 0.71 cm/s, GFAPCre$^{+/-}$IFNAR$^{fl/fl}$: 7.63 ± 0.54 cm/s; one-way ANOVA: F(3, 42) = 2.83, p = 0.0502; Figure 2B; activity: periphery, Ctrl: 86.66% ± 3.72%, NesCre$^{+/-}$IFNAR$^{fl/fl}$: 86.73% ± 1.90%, Syn1Cre$^{+/-}$IFNAR$^{fl/fl}$: 81.89% ± 6.08%, GFAPCre$^{+/-}$IFNAR$^{fl/fl}$: 87.50% ± 3.14%; center, Ctrl: 13.34% ± 3.72%, NesCre$^{+/-}$IFNAR$^{fl/fl}$: 13.26% ± 1.91%, Syn1Cre$^{+/-}$IFNAR$^{fl/fl}$: 18.10% ± 6.08%, GFAPCre$^{+/-}$IFNAR$^{fl/fl}$: 12.49% ± 3.14%; one-way ANOVA: F(3, 42) = 0.41, p = 0.74; Figure 2C).

Next, the learning ability of cell-type-selective IFNAR knockout mice was tested in the Morris water maze (Figures 2D and 2E). While NesCre$^{+/-}$IFNAR$^{fl/fl}$ and GFAPCre$^{+/-}$IFNAR$^{fl/fl}$ animals showed a learning impairment comparable to the full knockout, the learning performance of Syn1Cre$^{+/-}$IFNAR$^{fl/fl}$ mice was indistinguishable from that of the Ctrl animals (one-way ANOVA: $F_{Ctrl}(7, 96) = 11.39$, p < 0.0001; $F_{NesCre}(7, 104) = 0.97$, p = 0.45; $F_{Syn1Cre}(7, 88) = 4.06$, p = 0.0007; $F_{GFAPCre}(7, 64) = 0.92$, p = 0.49; $F_{Treatment}(3, 352) = 16.31$, p < 0.001; Figure 2D). Results of the reference memory tests showed that on probe trial day 6, the time spent by NesCre$^{+/-}$IFNAR$^{fl/fl}$ animals (32.39% ± 3.84%) in the TQ was significantly less than the Ctrl group (45.25 ± 4.25%, Fisher's LSD, p = 0.04, Figure 2E). No significant differences were observed for the time spent in the TQ between Syn1Cre$^{+/-}$IFNAR$^{fl/fl}$ and Ctrl mice (Fisher's LSD, day 6: p = 0.61, day 9: p = 0.24; Figure 2E). However, on probe trial day 9, Syn1Cre$^{+/-}$IFNAR$^{fl/fl}$ mice (52.59% ± 4.01%) spent significantly more time in the TQ compared to NesCre$^{+/-}$IFNAR$^{fl/fl}$ (37.59% ± 4.54%; Fisher's LSD, p = 0.01) and GFAPCre$^{+/-}$IFNAR$^{fl/fl}$ mice (33.01% ± 5.24%; Fisher's LSD, p = 0.007; Figure 2E). Subsequently, the evaluation of the respective search strategies (Figures S2A–S2D) displayed that the hippocampus-dependent search strategy increased over time, while hippocampus-independent search strategies decreased in the Ctrl and Syn1Cre$^{+/-}$IFNAR$^{fl/fl}$ groups (Figure S2B). This was not the case in NesCre$^{+/-}$IFNAR$^{fl/fl}$ and GFAPCre$^{+/-}$IFNAR$^{fl/fl}$ mice (two-way ANOVA: F(3, 352) = 10.53, p < 0.001; Figures S2C and S2D). These data show that expression of IFNAR on neuroectoderm-derived cells, specifically on astrocytes in the CNS, is required for normal spatial learning and memory formation. In line with this, the ablation of IFNAR signaling only in neurons did not affect spatial learning and memory formation.

In the next step, synaptic plasticity was analyzed. fEPSPs were recorded in conditional knockout and Ctrl mice. Here, basal synaptic transmission (two-way ANOVA: F(3, 444) = 2.24, p = 0.08; Figure S2E) and PPF were also not affected (two-way ANOVA: F(3, 444) = 2.41, p = 0.06; Figure S2F). In line with the learning impairment, slices derived from NesCre$^{+/-}$IFNAR$^{fl/fl}$ and GFAPCre$^{+/-}$IFNAR$^{fl/fl}$ mice exhibited a defect in LTP compared to Ctrl mice, whereas Syn1Cre$^{+/-}$IFNAR$^{fl/fl}$ mice displayed normal LTP (two-way ANOVA: F(3, 1480) = 359.1, p < 0.0001; Figure 2F). In addition, the mean value of the maintenance phase of LTP (T 75–80 min) was also significantly reduced in NesCre$^{+/-}$IFNAR$^{fl/fl}$ (1.15 ± 0.05, p < 0.0001) and GFAPCre$^{+/-}$IFNAR$^{fl/fl}$ (1.24 ± 0.07, p = 0.007) mice compared to the Ctrl (1.47 ± 0.04). Again, the mean value

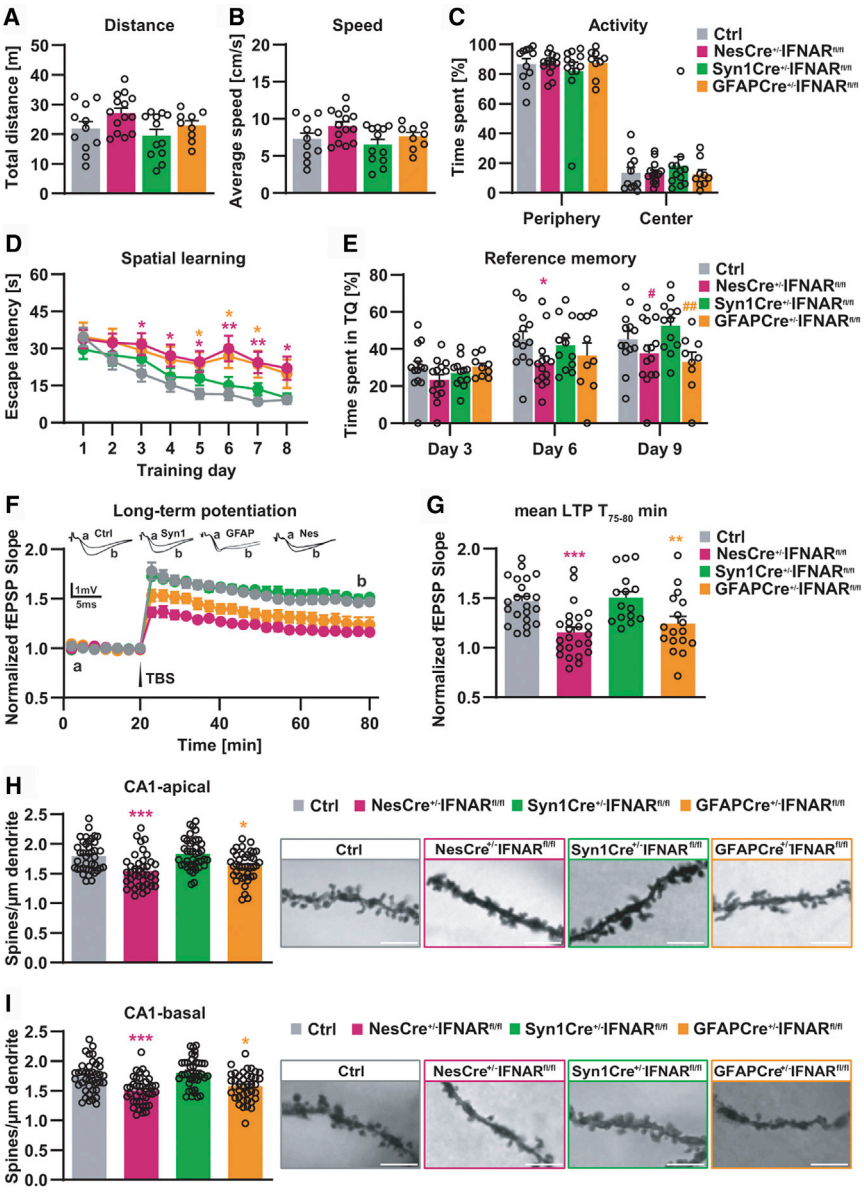

Figure 2. IFNAR Expression Specifically in Astrocytes Is Required for Normal Cognitive Function and Synaptic Plasticity

(A–C) Results of the open-field test showed unchanged (A) total distance traveled, (B) average speed, and (C) activity percentage in the periphery and center zones of the arena between cell-type-specific IFNAR knockout and respective Ctrl mice (n of mice in Ctrl = 11, NesCre$^{+/-}$IFNAR$^{fl/fl}$ = 14, Syn1Cre$^{+/-}$IFNAR$^{fl/fl}$ = 12, GFAPCre$^{+/-}$IFNAR$^{fl/fl}$ = 9).

(D) In the Morris water maze test, NesCre$^{+/-}$IFNAR$^{fl/fl}$ and GFAPCre$^{+/-}$IFNAR$^{fl/fl}$ mice showed higher escape latency than Ctrl animals (two-way ANOVA: $F(2, 264) = 19.88$, $p < 0.0001$); however, swimming time did not differ between Syn1Cre$^{+/-}$IFNAR$^{fl/fl}$ and Ctrl mice (two-way ANOVA: $F(1, 184) = 3.27$, $p = 0.07$).

(E) On day 6 of the probe trial tests, only NesCre$^{+/-}$IFNAR$^{fl/fl}$ mice spent significantly less time in the TQ compared to Ctrl animals. On probe trial day 9, both NesCre$^{+/-}$IFNAR$^{fl/fl}$ and GFAPCre$^{+/-}$IFNAR$^{fl/fl}$ mice showed lower preference for the TQ compared to Syn1Cre$^{+/-}$IFNAR$^{fl/fl}$ animals (n of mice in Ctrl = 13, NesCre$^{+/-}$IFNAR$^{fl/fl}$ = 14, Syn1Cre$^{+/-}$IFNAR$^{fl/fl}$ = 12, GFAPCre$^{+/-}$IFNAR$^{fl/fl}$ = 9).

(F) LTP was impaired in NesCre$^{+/-}$IFNAR$^{fl/fl}$ and GFAPCre$^{+/-}$IFNAR$^{fl/fl}$ mice but not in Syn1Cre$^{+/-}$IFNAR$^{fl/fl}$ animals.

(G) The mean LTP magnitude (T 75–80min) was significantly lower in NesCre$^{+/-}$IFNAR$^{fl/fl}$ and GFAPCre$^{+/-}$IFNAR$^{fl/fl}$ but not in Syn1Cre$^{+/-}$IFNAR$^{fl/fl}$ mice in comparison to Ctrl animals (n of slices in Ctrl = 22, NesCre$^{+/-}$IFNAR$^{fl/fl}$ = 24, Syn1Cre$^{+/-}$IFNAR$^{fl/fl}$ = 15, GFAPCre$^{+/-}$IFNAR$^{fl/fl}$ = 17).

(H and I) Spine density of (H) apical and (I) basal dendrites of CA1 hippocampal neurons was decreased in NesCre$^{+/-}$IFNAR$^{fl/fl}$ and GFAPCre$^{+/-}$IFNAR$^{fl/fl}$ mice compared to Ctrl animals. Spine density was not altered in Syn1Cre$^{+/-}$IFNAR$^{fl/fl}$ mice. Representative images show dendritic spines of hippocampal CA1 neurons in all tested groups (scale bar, 2 µm; n of mice in each group = 4, n of dendrites in each group = 40).

Data are presented as mean ± SEM. *$p < 0.05$, *$p < 0.01$, ***$p < 0.001$, compared to Ctrl. #$p < 0.05$ and ##$p < 0.01$, compared to Syn1Cre$^{+/-}$IFNAR$^{fl/fl}$.

of the maintenance phase of LTP in Syn1Cre$^{+/-}$IFNAR$^{fl/fl}$ mice (1.50 ± 0.06, $p = 0.70$) did not show any significant alterations compared to the Ctrl group (one-way ANOVA: $F(3, 74) = 8.76$, $p < 0.0001$; Figure 2G).

Moreover, significant reduction in the spine density of apical and basal dendrites of CA1 pyramidal neurons in NesCre$^{+/-}$IFNAR$^{fl/fl}$ (apical: Δ-13.95%, Tukey's test: $p = 0.0002$; basal: Δ-13.33%, Tukey's test: $p = 0.0003$) and GFAPCre$^{+/-}$IFNAR$^{fl/fl}$ mice (apical: Δ-9.31%, Tukey's test: $p = 0.022$; basal: Δ-9.18%, Tukey's test: $p = 0.023$) was observed, compared to the Ctrl group (Figures 2H and 2I). In line with LTP observations, no significant changes in apical and basal dendritic spine density were detected between Syn1Cre$^{+/-}$IFNAR$^{fl/fl}$ and Ctrl mice (apical: Δ+2.17%, Tukey's test: $p = 0.90$; basal: Δ+4.04%, Tukey's test: $p = 0.58$; Figures 2H and 2I). As for the full knockout, the conditional knockout mice displayed no signs of microgliosis (NesCre$^{+/-}$IFNAR$^{fl/fl}$, density: unpaired t test: $t = 0.30$, $df = 23$, $p = 0.76$; activity: unpaired t test: $t = 1.21$, $df = 23$, $p = 0.23$; GFAPCre$^{+/-}$IFNAR$^{fl/fl}$, density: unpaired t test: $t = 1.30$, $df = 38$, $p = 0.19$; activity: unpaired t test: $t = 0.66$, $df = 38$, $p = 0.51$; Figures S2G–S2I).

IFNAR Signaling Acutely Regulates Functional and Structural Synaptic Plasticity

Cell-type-specific IFNAR ablation showed that IFNAR signaling is involved in hippocampal synaptic plasticity and cognitive function in the healthy brain. To understand whether this might indeed be due to an acute role, we applied an IFNAR blocking antibody (10 µg/ml) or IgG1 κ isotype Ctrl antibody (10 µg/ml) on hippocampal slices (Figure 3). Following 1 h pre-treatment,

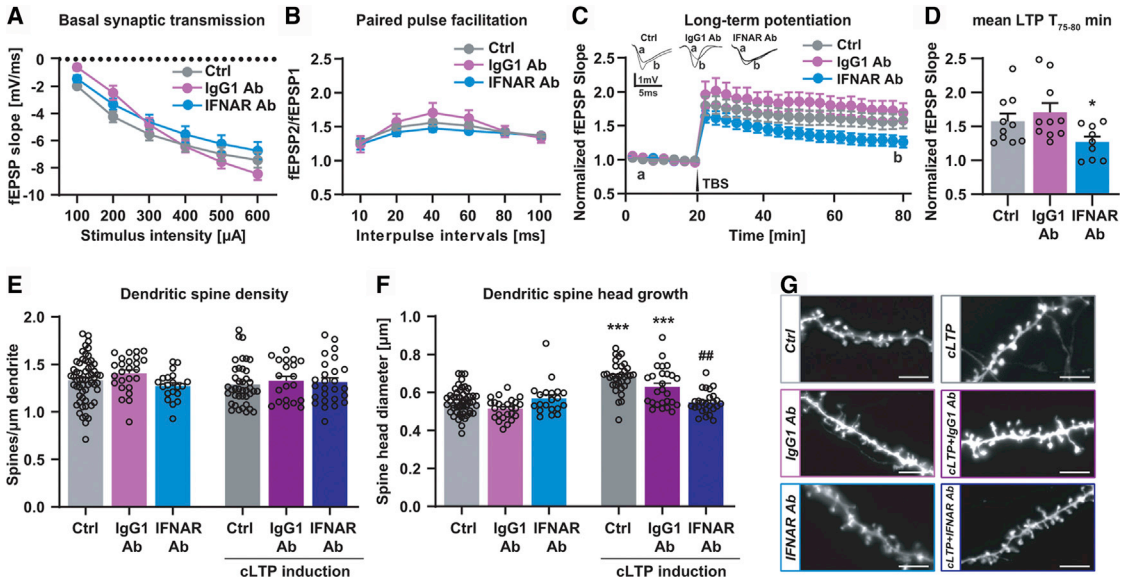

Figure 3. Acute Blocking of IFNAR Signaling Revealed a Direct Effect on Activity-Dependent Functional and Structural Synaptic Plasticity

(A) Input-output relationship (n of slices in Ctrl = 10, IgG1 Ab = 10, IFNAR Ab = 10), and (B) PPF were not altered in slices treated with the IFNAR blocking antibody, compared to IgG1-antibody-treated and untreated Ctrl slices (n of slices in Ctrl = 10, IgG1 Ab = 9, IFNAR Ab = 9).

(C) LTP was impaired in IFNAR-blocking-antibody-treated slices (n of slices in Ctrl = 10, IgG1 Ab = 10, IFNAR Ab = 9).

(D) The mean LTP magnitude (T 75–80 min) was lower in IFNAR-antibody-treated slices compared to IgG1-antibody-treated and untreated Ctrl slices.

(E) Spine density in IFNAR-blocking-antibody-treated compared to IgG1-antibody-treated and untreated Ctrl cells did not show any significant differences with and without cLTP induction (n of cells in Ctrl = 59, IgG1 Ab = 25, IFNAR Ab = 20, cLTP+Ctrl = 40, cLTP+IgG1 Ab = 20, cLTP+IFNAR Ab = 26).

(F) Spine-head diameter did not further increase following co-treatment of the IFNAR blocking antibody (10 μg/ml) and glycine and strychnine (cLTP), compared to IgG1-antibody-treated and untreated Ctrl slices (n of randomly selected spines per each dendrite = 20, n of cells in Ctrl = 52, IgG1 Ab = 25, IFNAR Ab = 20, cLTP+Ctrl = 33, cLTP+IgG1 Ab = 26, cLTP+IFNAR Ab = 26).

(G) Representative images of dendritic spines of hippocampal neurons in all tested groups (scale bar, 2 μm).

Data are presented as mean ± SEM. *p < 0.05, ***p < 0.001, compared to Ctrl and IgG1 Ab groups. ##p < 0.01, compared to Ctrl and IgG1 Ab groups after cLTP induction.

no significant difference in the fEPSP slope size was detected (two-way ANOVA F(2, 162) = 0.78, p = 0.46; Figure 3A). PPF was also not altered following the IFNAR blocking antibody treatment (two-way ANOVA F(2,150) = 0.48, p = 0.62; Figure 3B). In line with our data on *Ifnar*$^{-/-}$ mice, slices pre-treated with the IFNAR blocking antibody showed a significant impairment in LTP compared to the slices pre-treated with the Ctrl antibody and the untreated slices (two-way ANOVA F(2, 520) = 62.57, p < 0.0001; Figure 3C). Also, the mean value of the maintenance phase of LTP (last 5 min of recording) was significantly diminished in IFNAR-blocking-antibody-treated slices (1.26 ± 0.08), thereby revealing an impairment in synaptic plasticity, compared to the slices treated with the Ctrl antibody (1.70 ± 0.13, unpaired t test: t = 2.66, df = 17, p = 0.016) and the untreated slices (1.57 ± 0.11, unpaired t test: t = 2.16, df = 17, p = 0.045; Figure 3D). These results show that IFNAR signaling is acutely involved in functional synaptic plasticity under physiological conditions. Furthermore, we were interested in whether not only functional, but also structural, synaptic plasticity would be directly affected by IFNAR signaling. Therefore, LTP was induced chemically (cLTP) by using glycine and strychnine (Fortin et al., 2010) in primary embryonic hippocampal cultures treated with either the IFNAR blocking antibody (10 μg/ml) or the IgG1 κ isotype Ctrl antibody (10 μg/ml) (Figures 3E–3G). While dendritic spine density was not altered following the IFNAR blocking antibody treatment (one-way ANOVA F(5, 184) = 1.14, p = 0.33; Figure 3E), the observed activity-dependent spine-head enlargement after cLTP induction in Ctrl cells, compared to unstimulated Ctrl cells, was completely prevented by application of the IFNAR blocking antibody (unstimulated, Ctrl: 0.55 ± 0.009 μm; IgG1: 0.51 ± 0.01 μm; IFNAR Ab:0.56 ± 0.01 μm; cLTP, Ctrl: 0.68 ± 0.01 μm; IgG1: 0.62 ± 0.01 μm; IFNAR Ab: 0.54 ± 0.01 μm, one-way ANOVA: F(5, 176) = 20.69, p < 0.0001; Figures 3F and 3G). We can, therefore, show that both functional and structural plasticity are acutely dependent on IFNAR-mediated signaling pathways.

IFN-β Is Involved in Regulating Hippocampal Synaptic Plasticity

Since IFN-α is not present in the healthy CNS (Detje et al., 2009), IFN-β might be the major IFN involved in the homeostatic role of IFNAR signaling in the CNS described above. To confirm the role of IFN-β in cognitive function and synaptic plasticity under physiological conditions, *Ifnb*$^{-/-}$ animals were utilized (Figure 4). Analysis of the total distance traveled (Figure 4A) and average speed in the open field (Figure 4B) did not reveal any significant differences between *Ifnb*$^{-/-}$ and *WT* mice (distance, *WT*: 16.29 ± 1.66 m, *Ifnb*$^{-/-}$: 18.86 ± 1.49; unpaired t test: t = 1.09, df = 17, p = 0.28; speed,

CellPress
OPEN ACCESS

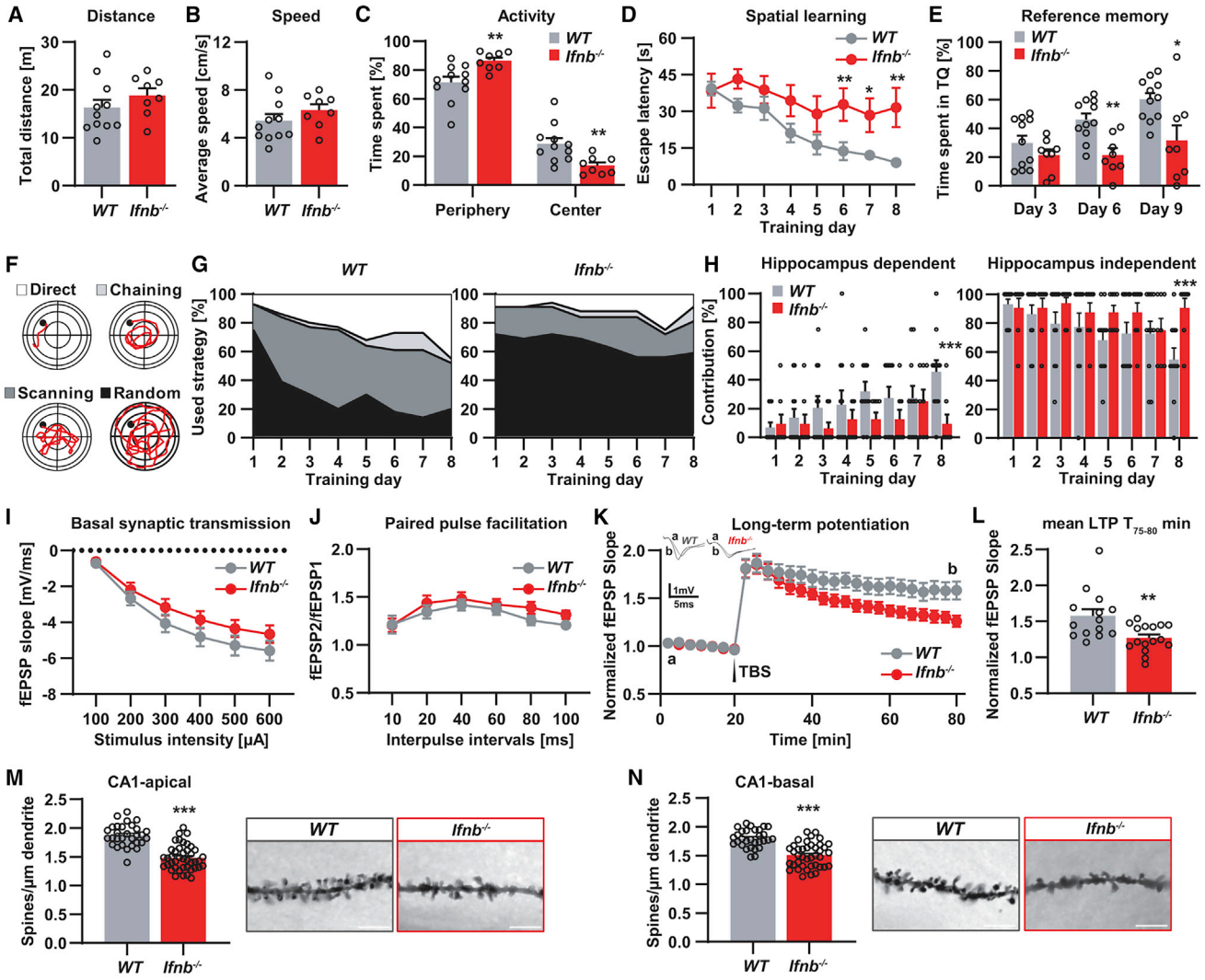

Figure 4. Impaired Cognitive Function and Synaptic Plasticity in *Ifnb*$^{-/-}$ Mice

(A and B) In *Ifnb*$^{-/-}$ mice, (A) total distance traveled and (B) average speed were not altered significantly compared to *WT* mice.

(C) *Ifnb*$^{-/-}$ mice exhibited more time spent in the periphery and less time spent in the center zone of the open-field arena. *Ifnb*$^{-/-}$ mice exhibited significantly increased anxiety-related behavior compared to *WT* mice (n of mice in *WT* = 11, *Ifnb*$^{-/-}$ = 8).

(D) In the Morris water maze test, *Ifnb*$^{-/-}$ mice showed higher escape latency and, therefore, impaired spatial learning compared to *WT* animals.

(E) On probe trials days 6 and 9, *Ifnb*$^{-/-}$ mice spent significantly less time in the TQ compared to *WT* animals.

(F) Example tracks of learning strategies used during the Morris water maze training.

(G) A reduction in the use of the hippocampus-dependent strategy by *Ifnb*$^{-/-}$ mice became apparent.

(H) Quantification of searching strategies showed that the hippocampus-dependent strategy was decreased, and hippocampus-independent strategies were increased in *Ifnb*$^{-/-}$ mice, compared to *WT* (n of mice in *WT* = 11, *Ifnb*$^{-/-}$ = 8).

(I) Basal synaptic transmission was not altered in both tested groups (n of slices in *WT* = 17, *Ifnb*$^{-/-}$ = 21).

(J) PPF was not different between *Ifnb*$^{-/-}$ and *WT* mice (n of slices in *WT* = 14, *Ifnb*$^{-/-}$ = 21).

(K) LTP was impaired in *Ifnb*$^{-/-}$ mice.

(L) The mean LTP magnitude (T 75–80 min) was lower in *Ifnb*$^{-/-}$ mice compared to *WT* mice (n of slices in *WT* = 14, *Ifnb*$^{-/-}$ = 16).

(M and N) Spine density of (M) apical and (N) basal dendrites of CA1 pyramidal hippocampal neurons was reduced in *Ifnb*$^{-/-}$ mice compared to *WT* mice. Representative images of dendritic spines of hippocampal CA1 neurons in both tested groups (scale bar, 2 µm; n of mice in *WT* = 3, *Ifnb*$^{-/-}$ = 4, n of dendrites in in *WT* = 30, *Ifnb*$^{-/-}$ = 40-42).

Data are presented as mean ± SEM. *p < 0.05, **p < 0.01, ***p < 0.001, compared to *WT*.

WT: 5.43 ± 0.56 cm/s, *Ifnb*$^{-/-}$: 6.31 ± 0.49 cm/s; unpaired t test: t = 1.11, df = 17, p = 0.27). However, *Ifnb*$^{-/-}$ mice spent significantly more time in the periphery and less time in the center zones of the open-field arena than the *WT* mice (periphery, *WT*: 71.41% ± 3.94%, *Ifnb*$^{-/-}$: 86.45% ± 2.21%; center, *WT*: 28.58% ± 3.94%, *Ifnb*$^{-/-}$: 13.55% ± 2.21%; unpaired

t test: t = 2.99, df = 17, p = 0.008; Figure 4C), indicating an increased anxiety-related behavior in *Ifnb*$^{-/-}$ mice.

Escape latency in the Morris water maze progressively diminished over 8 days of acquisition training in *WT* animals, but not in *Ifnb*$^{-/-}$ mice (one-way ANOVA: $F_{WT}(7, 80) = 11.39$, $p < 0.0001$ and $F_{Ifnb-/-}(7, 56) = 0.62$, $p = 0.73$). A day-by-day comparison of the data also showed a significantly higher escape latency during acquisition days 6–8 in *Ifnb*$^{-/-}$ mice compared to *WT* animals (two-way ANOVA: $F_{Treatment}(1, 136) = 28.01$, $p < 0.0001$, Fisher's LSD test - day 6: $p = 0.005$, day 7: $p = 0.017$, day 8: $p = 0.001$; Figure 4D). On probe trials days 6 (*WT*: 45.98% ± 4.22%, *Ifnb*$^{-/-}$: 21.42% ± 4.78%) and 9 (*WT*: 60.24% ± 4.36%, *Ifnb*$^{-/-}$: 31.58% ± 10.47%), *Ifnb*$^{-/-}$ mice spent significantly less time in the TQ compared to *WT* animals (day 6, unpaired t test: t = 3.82, df = 17, p = 0.0014; day 9, unpaired t test: t = 2.80, df = 17, p = 0.01; Figure 4E). Also, analysis of the searching strategies revealed that in *WT* mice, the use of the hippocampus-dependent and hippocampus-independent search strategies increased and decreased, respectively, over 8 days of acquisition training, whereas this was not the case for *Ifnb*$^{-/-}$ mice (Figures 4F and 4G). A quantification showed significantly fewer hippocampus-dependent (*WT*: 45.45% ± 8.13%, *Ifnb*$^{-/-}$: 9.37% ± 6.57%, Fisher's LSD: p = 0.0007) and more hippocampus-independent (*WT*: 54.54% ± 8.13%, IFN-β$^{-/-}$: 90.62% ± 6.57%, Fisher's LSD: p = 0.0007) searching strategies in *Ifnb*$^{-/-}$ mice compared to *WT*, especially on day 8 (Figure 4H). These findings revealed learning and memory deficits in *Ifnb*$^{-/-}$ mice.

As a next step, hippocampal synaptic plasticity was investigated to discover the potential cellular mechanisms responsible for this deficit (Figures 4I–4L). While *Ifnb*$^{-/-}$ mice showed no impairments in baseline synaptic transmission (two-way ANOVA: $F(1, 216) = 1.47$, $p = 0.23$; Figure 4I) or PPF (two-way ANOVA: $F(1, 198) = 0.80$, $p = 0.37$; Figure 4J), LTP was significantly impaired in *Ifnb*$^{-/-}$ animals (two-way ANOVA: $F(1, 560) = 60.39$, $p < 0.0001$; Figure 4K). A reduced mean value of LTP (T 75–80 min) in *Ifnb*$^{-/-}$ mice (1.27 ± 0.046) was observed compared to in *WT* (1.57 ± 0.09, unpaired t test: t = 3.094, df = 28, p = 0.004; Figure 4L). In addition, a significant reduction in the spine density of apical and basal dendrites of CA1 pyramidal neurons (Figures 4M and 4N) in *Ifnb*$^{-/-}$ mice, compared to *WT* animals, was detected (apical: Δ-20.92%, unpaired t test: t = 7.97, df = 70, p < 0.0001; basal: Δ-16.14% unpaired t test: t = 6.34, df = 68, p < 0.0001).

Next, in a gain-of-function approach, we applied IFN-β at a low dose (1000 U/ml) with and without cLTP induction in primary embryonic hippocampal cultures, as described above (Figures 5A–5C). Again, a significant difference in spine density was not detected among all tested groups (one-way ANOVA: $F(3, 116) = 2.55$, $p = 0.06$; Figure 5A). cLTP induction resulted in a highly significant increase in spine-head diameter in the cLTP Ctrl group (0.62 ± 0.01 μm) compared to the untreated Ctrl cells (0.48 ± 0.008 μm, Tukey's test: p < 0.0001). The application of IFN-β together with cLTP induction did not lead to a significant further increase in spine-head diameter (0.67 ± 0.01 μm) compared to cLTP induction alone (Tukey's test: p = 0.12). Yet, the application of IFN-β already under baseline conditions significantly increased spine-head size (0.60 ± 0.01 μm, Tukey's test: p < 0.0001), comparable to that observed after cLTP induction (one-way ANOVA: $F(3, 116) = 44.34$, $p < 0.0001$; Figures 5B and 5C). These results suggest that a low-dose application of IFN-β in a physiological range is sufficient to induce spine structural plasticity. Next, to investigate whether the effect of the IFN-β application is indeed IFNAR specific, primary embryonic hippocampal cultures obtained from *Ifnar*$^{-/-}$ mice were treated with IFN-β (1000 U/ml) alone or together with glycine and strychnine (cLTP induction) (Figures 5D–5F). Results did not reveal any significant differences in spine density (one-way ANOVA: $F(3, 116) = 1.25$, $p = 0.29$; Figure 5D) or in spine-head diameter (one-way ANOVA: $F(3, 116) = 1.12$, $p = 0.34$; Figure 5E) among all experimental groups. Moreover, similar spine-head diameter in both unstimulated (0.50 ± 0.01 μm) and stimulated (0.49 ± 0.01 μm, Tukey's test: p = 0.90) *Ifnar*$^{-/-}$ cultures with glycine and strychnine indicated impaired cLTP induction in *Ifnar*$^{-/-}$ neurons, which was in line with our *in vivo* observations (Figure 1). As the activity-dependent spine-head enlargement following cLTP induction is mediated by glutamate receptors, we were interested in understanding whether IFNAR-mediated effects on structural synaptic plasticity were dependent on ionotropic glutamate receptors. Therefore, primary embryonic hippocampal cultures obtained from *WT* mice were treated with IFN-β alone or together with APV (D-2-amino-5-phosphonovalerate) and CNQX (6-Cyano-7-nitroquinoxaline-2,3-dione disodium) (ionotropic glutamate receptor inhibitors [iGluR Is]; Figures 5G–5I). Spine density was not altered in all groups tested (one-way ANOVA: $F(2, 62) = 0.16$, $p = 0.85$; Figure 5G). However, IFN-β treatment (0.62 ± 0.01 μm) led to a significant increase in spine-head diameter compared to the Ctrl cells (0.52 ± 0.008 μm, Tukey's test: p < 0.0001). Blocking the NMDA receptor (NMDAR) and AMPA receptor (AMPAR) by APV and CNQX inhibited the IFN-β mediated increase in dendritic spine-head diameter (0.55 ± 0.01 μm, Tukey's test: p = 0.31; Figures 5H and 5I). These findings suggest that synaptic plasticity induced by low levels of IFN-β is dependent on iGluRs. In conclusion, IFN-β regulates spine plasticity by inducing structural changes in dendritic spines via iGluRs.

IFNAR Signaling Regulates GLAST Expression on Astrocytes to Modulate Hippocampal Synaptic Plasticity

Our *in vivo* experiments revealed that astrocytes are the main cell type involved in IFNAR-mediated effects on synaptic plasticity; therefore, we were interested in the pathways that might be involved in modulating neuron-glia crosstalk in this scenario. Previously, it was shown that IFN-β can alter astrocyte-specific GLAST expression (Costello and Lynch, 2013). Therefore, we investigated whether the expression of GLAST would be regulated following IFN-β treatment in primary embryonic hippocampal cultures (Figures 6A and 6B). Anti-GLAST immunostaining revealed that a low-dose application of IFN-β (1000 U/ml) led to a significant reduction in the expression level of GLAST in astrocytes (20.25% ± 2.45%) in primary embryonic hippocampal cultures compared to untreated cultures (29.83% ± 2.85%, Fisher's LSD: p = 0.025). On the other hand, GLAST expression was elevated significantly following application of the IFNAR blocking antibody (39.7% ± 5.09%, Fisher's LSD: p = 0.049; Figures 6A and 6B). As a next step, GLAST expression was determined in

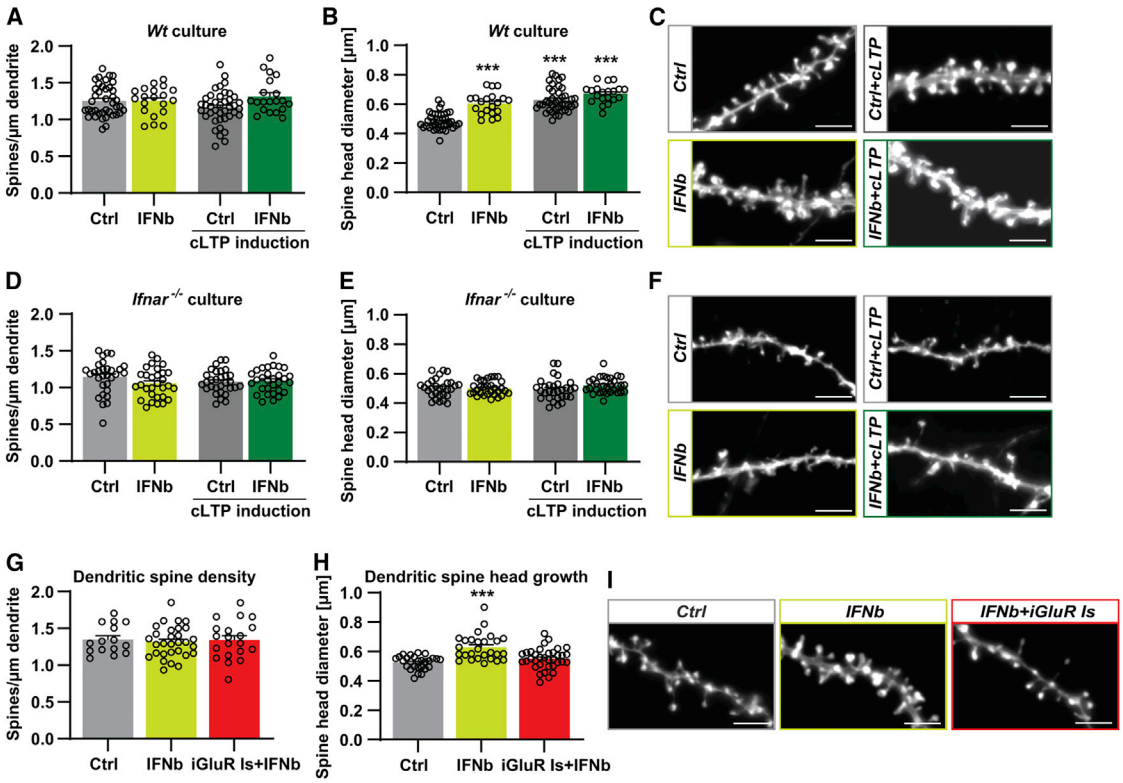

Figure 5. Low-Dose IFN-β Application Induces Positive Spine Structural Plasticity

(A and B) Upon IFN-β (1000 U/ml) treatment of primary embryonic hippocampal cultures derived from *WT* mice for 10 min (A) assessment of spine density in all treatments compared to untreated cells (Ctrl) did not show any significant differences. (B) IFN-β (1000 U/ml) treatment led to a significant increase in dendritic spine-head diameter. Co-treatment of IFN-β together with cLTP induction revealed no additional spine-head growth.

(C) Representative images of dendritic spines of hippocampal neurons in all treated cells derived from *WT* mice (scale bar, 2 μm; n of cells in Ctrl = 40, IFN-β = 20, cLTP+Ctrl = 40, cLTP+IFN-β = 20, n of randomly selected spines per each dendrite = 20).

(D and E) IFN-β (1000 U/ml) treatment of primary embryonic hippocampal cultures derived from *Ifnar*$^{-/-}$ mice alone or together with cLTP for 10 min did not show any significant differences in (D) dendritic spine density and (E) head diameter.

(F) Representative images of dendritic spines of hippocampal neurons in all treated cells derived from *Ifnar*$^{-/-}$ mice (scale bar, 2 μm; n of cells in each group = 30, n of randomly selected spines per each dendrite = 20).

(G and H) The administration of 1000 U/ml IFN-β alone or accompanied by APV and CNQX did not alter dendritic spine density; however, (H) co-application of IFN-β and ionotropic glutamate receptor inhibitors (iGluR Is) showed that the positive effect of IFN-β on spine-head diameter is dependent on ionotropic glutamate receptor signaling.

(I) Representative images of dendritic spines of hippocampal neurons in all tested groups (scale bar, 2 μm; n of cells in Ctrl = 15, IFN-β = 30, IFN-β+iGluR Is = 20 n of randomly selected spines per each dendrite = 20).

Data are presented as mean ± SEM. ***p < 0.001, compared to *Ctrl*.

the hippocampus of conventional and conditional IFNAR knockout mice using immunohistochemistry (Figures 6C and 6D) and western blotting (Figure 6E). While no alterations in GLAST expression were observed in the Syn1Cre$^{+/-}$IFNAR$^{fl/fl}$ mice (immunostaining: Δ-0.76%, Fisher's LSD: p = 0.93; western blotting: Δ+6.6%, Fisher's LSD: p = 0.87), GLAST levels were significantly increased in the hippocampus of *Ifnar*$^{-/-}$ (immunostaining: Δ+26%, Fisher's LSD: p = 0.005; western blotting: Δ+189.6%, Fisher's LSD: p < 0.0001), NesCre$^{+/-}$IFNAR$^{fl/fl}$ (immunostaining: Δ+21%, Fisher's LSD: p = 0.023; western blotting: Δ+190.2%, Fisher's LSD: p < 0.0001), and GFAPCre$^{+/-}$IFNAR$^{fl/fl}$ mice (immunostaining: Δ+41.7%, Fisher's LSD: p < 0.0001; western blotting: Δ+204.5%, Fisher's LSD: p < 0.0001) compared to *WT* animals (Figures 6C–6E). These findings suggest that dysregulation of glutamate homeostasis, following IFNAR ablation specifically in astrocytes, may be at least partly responsible for impaired hippocampal synaptic plasticity. Additional evidence comes from experiments where we partially blocked GLAST activity by application of a glutamate transporter inhibitor (TFB-TBOA), which indeed mimicked the positive effects of low concentrations of IFN-β on spine structural plasticity (Figures 6F and 6G). TFB-TBOA is a selective inhibitor of glutamate transporters EAAT1, EAAT2, and EAAT3 in glial cells (Bozzo and Chatton, 2010). While no significant differences in dendritic spine density were detected among the different treated groups (one-way ANOVA: F(3, 88) = 1.24, p = 0.29; Figure 6F), administration of TFB-TBOA alone (0.55 ± 0.01 μm, Tukey's test: p = 0.0002) or accompanied by cLTP induction (0.53 ± 0.01 μm, Tukey's test: p = 0.01) led to a significant elevation in dendritic spine-head diameter compared to untreated Ctrl

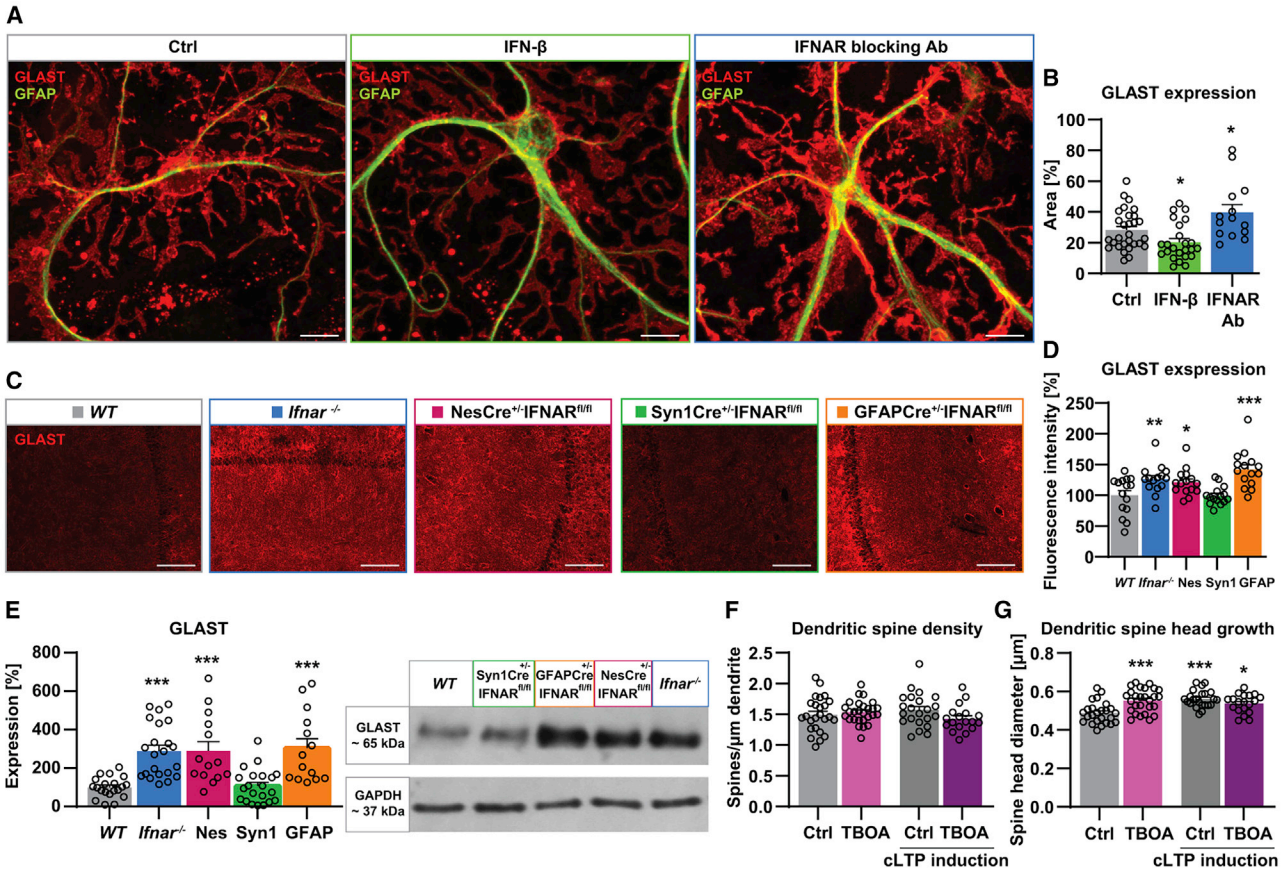

Figure 6. Signaling of IFN-β via the IFNAR in Astrocytes Involves Modulation of the Glutamate Transporter GLAST

(A) Representative examples of anti-GLAST and anti-GFAP immunostaining in primary embryonic hippocampal cultures (scale bar, 10 μm).

(B) Anti-GLAST immunocytochemistry in primary embryonic hippocampal cultures showed a significant reduction or elevation in GLAST expression levels following application of IFN-β (1000 U/ml) or IFNAR blocking antibody (10 μg/ml), respectively (n of cells in Ctrl = 30, IFN-β = 24, IFNAR Ab = 14).

(C) Representative examples of anti-GLAST immunohistochemistry in the CA1 region of *WT*, conventional, and conditional IFNAR knockout mice (scale bar, 50 μm).

(D) GLAST expression was higher in the CA1 hippocampal subregion of *Ifnar*$^{-/-}$, NesCre$^{+/-}$IFNAR$^{fl/fl}$, and GFAPCre$^{+/-}$IFNAR$^{fl/fl}$, but not of Syn1Cre$^{+/-}$IFNAR$^{fl/fl}$ mice, compared to *WT* animals (n of mice in each group = 3, n of ROIs per each mouse = 5).

(E) In addition, GLAST expression was determined by western immunoblot, and values were normalized to GAPDH. Here as well, GLAST expression was significantly increased in the hippocampus of *Ifnar*$^{-/-}$, NesCre$^{+/-}$IFNAR$^{fl/fl}$, and GFAPCre$^{+/-}$IFNAR$^{fl/fl}$, but not in Syn1Cre$^{+/-}$IFNAR$^{fl/fl}$ mice, compared to respective Ctrl animals (n of samples in *WT* = 20, NesCre$^{+/-}$IFNAR$^{fl/fl}$ = 22, Syn1Cre$^{+/-}$IFNAR$^{fl/fl}$ = 15, GFAPCre$^{+/-}$IFNAR$^{fl/fl}$ = 21). Insets illustrate representative blots of GLAST along with respective GAPDH blots.

(F and G) Upon TFB-TBOA (20 nM) treatment of primary embryonic hippocampal cultures for 10 min (F) spine density in all treatments compared to untreated Ctrl cells did not show any significant differences. (G) TFB-TBOA (20 nM) treatment led to a significant elevation in dendritic spine-head diameter. Treatment of TFB-TBOA (20 nM) and cLTP induction did not lead to an additional spine-head increase. n of cells in Ctrl = 25, TBOA = 27, cLTP+Ctrl = 22, cLTP+TBOA = 18.

Data are presented as mean ± SEM. *p < 0.05, **p < 0.01, ***p < 0.001, compared to *WT* (A–E) and (F and G) Ctrl.

cells (0.48 ± 0.01 μm, one-way ANOVA: F(3, 90) = 9.53, p < 0.0001; Figure 6G). In summary, we can show with our *in vitro* data that IFNAR signaling leads to structural spine-head plasticity by decreasing astrocytic glutamate uptake.

DISCUSSION

The most important cytokines involved in brain-immune interaction both under physiological and pathological conditions are interleukins (ILs), tumor necrosis factor alpha (TNF-α), and IFNs. IFN-α and IFN-β are the predominant type I IFNs in the CNS, so far mostly implicated as important mediators of antiviral immune responses. All CNS cell types, including neurons and glial cells, are able to produce and respond to IFNs (Owens et al., 2014). Earlier studies revealed that immune-deficient mice are more susceptible to mental stress, suffer from cognitive deficits, and show reduced levels of hippocampal neurogenesis when compared to their *WT* counterparts (Deczkowska et al., 2016; Ziv et al., 2006). The hippocampus is a highly plastic brain region, involved in learning and memory formation, which are especially sensitive to cytokines (Hosseini et al., 2018; Korte and Schmitz, 2016). In this study, we were therefore interested in a possible

physiological role of IFNAR signaling for cognitive function in general and for learning and memory formation in particular. For this purpose, conventional as well as different conditional knockout mouse lines for IFNAR signaling were investigated. Interestingly, IFNAR ablation led to a strong impairment in memory formation in conventional *Ifnar*$^{-/-}$ mice, which was associated with deficits in hippocampal LTP and reduced dendritic spine density. Memory retrieval during probe trials in the Morris water maze, however, was only mildly impaired, suggesting that other areas in the CNS, like parts of the neocortex, might be less affected than the highly vulnerable hippocampal CA1 region. It needs to be emphasized that no signs of microgliosis in the absence of IFNAR could be detected. Further detailed analysis might be used in the future to determine whether there would be more subtle signs of microgliosis and astrogliosis in this context. The strong impairments in synaptic plasticity, synapse number, and memory formation imply that IFNAR signaling is also involved in brain function in the absence of viral infection under physiological states. This phenomenon has been also described for other cytokines, including IL-1β and TNF-α (McAfoose and Baune, 2009; Santello et al., 2011). We next addressed which cell types would be the most important IFN responders. While a pure neuronal knockout did not recapitulate the phenotype observed in *Ifnar*$^{-/-}$ mice, IFNAR loss specifically in astrocytes almost completely mimicked the phenotype.

Cognitive impairments might partly result from developmental alterations in neuronal network formation in the absence of IFNAR signaling. It was indeed shown previously that astrocytes release glutamate, ATP, and cytokines such as TNF-α and type I IFN that change the survival rate and function of newly formed connections between neurons (Ota et al., 2013). Furthermore, it has been shown that cytokines such as IFN are able to control neurogenesis and brain development by modulating growth, differentiation, and survival of neuronal cells (Mehler and Kessler, 1998). For instance, IFN-treated fetal murine neuroblast cultures developed a differentiated neuronal population associated with the expression of mature neurofilament proteins (Plioplys, 1988). In addition, JAK-STAT signaling downstream of many cytokines, such as type I IFN and IL-2, IL-6, IL-10, and TNF-α (Murray, 2007), plays a critical role in various brain developmental pathways, especially in promoting astrogliogenesis (Lee et al., 2016). Astrocytes, in turn, are known to substantially contribute to CNS development by controlling synaptogenesis and axon guidance factors (Chung et al., 2015b). During development, astrocytes release and respond to other factors such as brain-derived neurotrophic factor (BDNF), transforming growth factor β (TGF-β), and thrombospondin (TSP), thereby controlling glutamatergic synapse formation (Chung et al., 2015b). Previously, it was shown that in Down syndrome, elevated IFN-γ levels are associated with a reduction in TSP-1 secretion from astrocytes (Garcia et al., 2010). Therefore, physiological levels of IFNAR signaling and subsequent activation of JAK-STAT pathways might be important for astrocyte maturation and function, which in turn could regulate neuronal network development and function (de Araujo et al., 2009). In addition to the possible chronic effect of IFNAR loss on neuronal network formation, our data presented here provide evidence for a direct and acute effect of IFNAR signaling on synaptic plasticity and hippocampal function. Previously, it was shown that cytokines are able to exert neuroprotective effects (Carlson et al., 1999). Thus, elucidation of the detailed mechanisms by which immune molecules can affect neuronal function has important implications to understand the balance between beneficial effects during normal brain function and adverse effects of cytokine signaling during processes of inflammation. There is indeed evidence for the contribution of cytokines to the acquisition, consolidation, and retrieval of memories (Donzis and Tronson, 2014). For instance, several studies revealed an important role for IL-1β for hippocampus-dependent memory formation. The levels of IL-1β are reported to increase during LTP induction or following context-dependent fear conditioning, suggesting a critical role of this cytokine in learning and memory formation (Schneider et al., 1998). In addition, it has been shown that low levels of IL-1β have a physiological role in the maintenance phase of LTP, whereas high pathological concentrations inhibit LTP (Schneider et al., 1998). The levels of TNF-α were also shown to increase after learning; however, this cytokine seems not to be directly important for learning and memory consolidation (Belarbi et al., 2012). Recent studies showed that TNF-α released from astrocytes can act as a gliotransmitter by promoting the membrane insertion of α-amino-3-hydroxy-5-methyl-4-isoxazolepropionic acid (AMPA) receptors in neurons (Theodosis et al., 2008). Therefore, the constitutive release of physiological levels of TNF-α contributes to the homeostatic activity-dependent regulation of synaptic connectivity (Stellwagen and Malenka, 2006). IFNs can also act as neuromodulators, which are able to exert direct effects on synaptic transmission and function (Costello and Lynch, 2013; Hadjilambreva et al., 2005). Differential signaling outcomes of IFN-α and IFN-β can determine whether type I IFN exert pathogenic or protective roles in the CNS, depending on their concentration (Owens et al., 2014). Using hippocampal slices, we showed here that blocking IFNAR acutely resulted in impairments in functional and structural plasticity. Moreover, a low-dose application of IFN-β alone, as a major ligand for IFNAR, was already sufficient to induce spine-head plasticity. In line with this, we showed impaired spatial memory formation and LTP, as well as reduced dendritic spine density in adult *Ifnb*$^{-/-}$ mice. Indeed, it was previously reported that these mice show behavioral and cognitive impairments as well as neurodegeneration later in life (Ejlerskov et al., 2015). Our results, therefore, indicate a direct role of IFNAR signaling in astrocytes for synaptic plasticity and cognitive function. It could be shown previously that conditional astrocyte-specific IL-1 receptor knockout mice display memory deficits (Ben Menachem-Zidon et al., 2011). A possible mechanism might be the regulation of available glutamate in the synaptic cleft by glutamate transporters GLT-1 and GLAST, which indeed have been shown to promote LTP (Swanson, 2005). Previously, it was reported that by releasing and responding to different cytokines such as TNF-α, CCL2, and IL-1, astrocytes are involved in different aspects of synaptic plasticity by regulating glutamate transport at the synapse, as well as the insertion of AMPA receptors and inhibition of NMDA receptor activity (Ota et al., 2013). It was shown that constitutive TNF-α in the hippocampus, specifically in the dentate gyrus, activates astrocyte P2Y1 receptors and subsequently induces localized Ca^{2+} elevations, followed by glutamate

release and presynaptic NMDA receptor-dependent synaptic potentiation (Santello et al., 2011). Here, we showed that a low-dose application of IFN-β or the IFNAR blocking antibody led to a decrease or increase, respectively, in astrocytic GLAST expression, suggesting that glutamate uptake modulation might directly affect synaptic activity. In addition, the treatment of hippocampal cultures with TFB-TBOA as a selective inhibitor of glial glutamate transporters mimicked the positive effects of low concentrations of IFN-β on spine structural plasticity. Therefore, the regulation of astrocytic glutamate transports, and thereby available glutamate at the synapse, may represent a possible mechanism by which type I IFNs are involved in directly modulating synaptic plasticity and cognitive function.

Taken together, this study shows that in the absence of viral infection, IFNAR signaling, most likely by modulating neuron-astrocyte crosstalk, is crucial for synapse numbers as well as synaptic plasticity and cognitive function. We provide evidence that IFNAR signaling at physiological levels regulates GLAST expression in astrocytes and thereby might represent a crucial mechanism to modulate neuronal excitability during synaptic plasticity (Chung et al., 2015a). However, because microglia are one of the major type-I-IFN-producing cells and, at the same time, are also highly responsive to it (Goldmann et al., 2016), we cannot ignore the importance of microglia in IFNAR signaling for controlling brain homeostasis and function. Interestingly, phenotypes such as anxiety-related behavior in *Ifnb*$^{-/-}$ mice and hyperactivity or the strongest reduction in dendritic spine number were detectable only in conventional IFNAR knockout mice, but not in mice showing a neuroectodermal cell-selective IFNAR deletion, suggesting that IFNAR triggering of some other CNS-resident cell type accounts for these effects. The findings of this study are also of special interest, as type I IFN inhibitors are used for therapeutic purposes in patients with lupus or other severe inflammatory diseases. Inhibition of high levels of type I IFNs in the brains of these patients might present a new therapeutic strategy for preventing possible CNS disorders caused by increased levels of IFN (McGlasson and Hunt, 2017). However, the results of this study indicate that the therapeutic inhibition of IFNAR signaling in the brain might not be without potential consequences, given the pivotal role of this pathway in host defense and the importance of basal levels of IFNAR signaling for synaptic plasticity described here under physiological conditions.

STAR★METHODS

Detailed methods are provided in the online version of this paper and include the following:

- KEY RESOURCES TABLE
- RESOURCE AVAILABILITY
  - Lead Contact
  - Materials Availability
  - Data and Code Availability
- EXPERIMENTAL MODEL AND SUBJECT DETAILS
  - Mice
  - Primary embryonic hippocampal culture
  - Acute mouse hippocampal slices
- METHOD DETAILS
  - Behavioral assays
  - Electrophysiological experiments
  - Golgi-Cox staining
  - Transfection
  - Chemical LTP (cLTP) induction in primary embryonic hippocampal culture
  - Immunohistochemistry
  - Immunocytochemistry
  - Imaging and image analysis
  - Western Immunoblotting
- QUANTIFICATION AND STATISTICAL ANALYSIS

SUPPLEMENTAL INFORMATION

Supplemental Information can be found online at https://doi.org/10.1016/j.celrep.2020.107666.

ACKNOWLEDGMENTS

M.K. and U.K. are funded by the Helmholtz-Gemeinschaft, Zukunftsthema "Immunology and Inflammation" (ZT-0027); M.K. is funded by the DFG (SFB854, TP25). U.K. and M.K. were supported by a bilateral project of the German Center for Neurodegenerative Diseases and the Helmholtz Centre for Infection Research. We thank Diane Mundil for excellent technical assistance in the cell culture.

AUTHOR CONTRIBUTIONS

Conceptualization, M.K., U.K., and K.M.-P.; Funding Acquisition, M.K. and U.K.; Performed the Experiments, S.H. and G.G.; Formal Analysis of the Data, S.H., K.M.-P., and G.G.; Resources, M.K. and U.K.; Writing –Original Draft, S.H., K.M.-P., M.K.; Writing – Review & Editing, S.H., K.M.-P., M.K., U.K., and C.C.

DECLARATION OF INTERESTS

The authors declare no competing interests.

Received: August 2, 2019
Revised: January 23, 2020
Accepted: April 28, 2020
Published: May 19, 2020

REFERENCES

Bajenaru, M.L., Zhu, Y., Hedrick, N.M., Donahoe, J., Parada, L.F., and Gutmann, D.H. (2002). Astrocyte-specific inactivation of the neurofibromatosis 1 gene (NF1) is insufficient for astrocytoma formation. Mol. Cell. Biol. *22*, 5100–5113.

Belarbi, K., Jopson, T., Tweedie, D., Arellano, C., Luo, W., Greig, N.H., and Rosi, S. (2012). TNF-α protein synthesis inhibitor restores neuronal function and reverses cognitive deficits induced by chronic neuroinflammation. J. Neuroinflammation *9*, 23.

Ben Menachem-Zidon, O., Avital, A., Ben-Menahem, Y., Goshen, I., Kreisel, T., Shmueli, E.M., Segal, M., Ben Hur, T., and Yirmiya, R. (2011). Astrocytes support hippocampal-dependent memory and long-term potentiation via interleukin-1 signaling. Brain Behav. Immun. *25*, 1008–1016.

Blank, T., and Prinz, M. (2017). Type I interferon pathway in CNS homeostasis and neurological disorders. Glia *65*, 1397–1406.

Bozzo, L., and Chatton, J.Y. (2010). Inhibitory effects of (2S, 3S)-3-[3-[4-(trifluoromethyl)benzoylamino]benzyloxy]aspartate (TFB-TBOA) on the astrocytic sodium responses to glutamate. Brain Res. *1316*, 27–34.

Carlson, N.G., Wieggel, W.A., Chen, J., Bacchi, A., Rogers, S.W., and Gahring, L.C. (1999). Inflammatory cytokines IL-1 α, IL-1 β, IL-6, and TNF-α impart neuroprotection to an excitotoxin through distinct pathways. J. Immunol. *163*, 3963–3968.

Chhatbar, C., Detje, C.N., Grabski, E., Borst, K., Spanier, J., Ghita, L., Elliott, D.A., Jordao, M.J.C., Mueller, N., Sutton, J., et al. (2018). Type I Interferon Receptor Signaling of Neurons and Astrocytes Regulates Microglia Activation during Viral Encephalitis. Cell Rep *25*, 118–129.e114.

Chung, W.-S., Welsh, C.A., Barres, B.A., and Stevens, B. (2015a). Do glia drive synaptic and cognitive impairment in disease? Nat. Neurosci. *18*, 1539–1545.

Chung, W.S., Allen, N.J., and Eroglu, C. (2015b). Astrocytes Control Synapse Formation, Function, and Elimination. Cold Spring Harb. Perspect. Biol. *7*, a020370.

Costello, D.A., and Lynch, M.A. (2013). Toll-like receptor 3 activation modulates hippocampal network excitability, via glial production of interferon-β. Hippocampus *23*, 696–707.

Crow, Y.J., and Manel, N. (2015). Aicardi-Goutières syndrome and the type I interferonopathies. Nat. Rev. Immunol. *15*, 429–440.

D'Arcangelo, G., Grassi, F., Ragozzino, D., Santoni, A., Tancredi, V., and Eusebi, F. (1991). Interferon inhibits synaptic potentiation in rat hippocampus. Brain Res. *564*, 245–248.

de Araujo, E.G., da Silva, G.M., and Dos Santos, A.A. (2009). Neuronal cell survival: the role of interleukins. Ann. N Y Acad. Sci. *1153*, 57–64.

Deczkowska, A., Baruch, K., and Schwartz, M. (2016). Type I/II interferon balance in the regulation of brain physiology and pathology. Trends Immunol. *37*, 181–192.

Detje, C.N., Meyer, T., Schmidt, H., Kreuz, D., Rose, J.K., Bechmann, I., Prinz, M., and Kalinke, U. (2009). Local type I IFN receptor signaling protects against virus spread within the central nervous system. J. Immunol. *182*, 2297–2304.

Detje, C.N., Lienenklaus, S., Chhatbar, C., Spanier, J., Prajeeth, C.K., Soldner, C., Tovey, M.G., Schlüter, D., Weiss, S., Stangel, M., and Kalinke, U. (2015). Upon intranasal vesicular stomatitis virus infection, astrocytes in the olfactory bulb are important interferon Beta producers that protect from lethal encephalitis. J. Virol. *89*, 2731–2738.

Donzis, E.J., and Tronson, N.C. (2014). Modulation of learning and memory by cytokines: signaling mechanisms and long term consequences. Neurobiol. Learn. Mem. *115*, 68–77.

Ejlerskov, P., Hultberg, J.G., Wang, J., Carlsson, R., Ambjørn, M., Kuss, M., Liu, Y., Porcu, G., Kolkova, K., Friis Rundsten, C., et al. (2015). Lack of Neuronal IFN-β-IFNAR Causes Lewy Body- and Parkinson's Disease-like Dementia. Cell *163*, 324–339.

Erlandsson, L., Blumenthal, R., Eloranta, M.L., Engel, H., Alm, G., Weiss, S., and Leanderson, T. (1998). Interferon-beta is required for interferon-alpha production in mouse fibroblasts. Curr. Biol. *8*, 223–226.

Fensterl, V., Chattopadhyay, S., and Sen, G.C. (2015). No Love Lost Between Viruses and Interferons. Annu. Rev. Virol. *2*, 549–572.

Fortin, D.A., Davare, M.A., Srivastava, T., Brady, J.D., Nygaard, S., Derkach, V.A., and Soderling, T.R. (2010). Long-term potentiation-dependent spine enlargement requires synaptic Ca2+-permeable AMPA receptors recruited by CaM-kinase I. J. Neurosci. *30*, 11565–11575.

Garcia, O., Torres, M., Helguera, P., Coskun, P., and Busciglio, J. (2010). A role for thrombospondin-1 deficits in astrocyte-mediated spine and synaptic pathology in Down's syndrome. PLoS ONE *5*, e14200.

Garthe, A., and Kempermann, G. (2013). An old test for new neurons: refining the Morris water maze to study the functional relevance of adult hippocampal neurogenesis. Front. Neurosci. *7*, 63.

Garthe, A., Behr, J., and Kempermann, G. (2009). Adult-generated hippocampal neurons allow the flexible use of spatially precise learning strategies. PLoS ONE *4*, e5464.

Goldmann, T., Blank, T., and Prinz, M. (2016). Fine-tuning of type I IFN-signaling in microglia–implications for homeostasis, CNS autoimmunity and interferonopathies. Curr. Opin. Neurobiol. *36*, 38–42.

Gough, D.J., Messina, N.L., Hii, L., Gould, J.A., Sabapathy, K., Robertson, A.P., Trapani, J.A., Levy, D.E., Hertzog, P.J., Clarke, C.J., and Johnstone, R.W. (2010). Functional crosstalk between type I and II interferon through the regulated expression of STAT1. PLoS Biol. *8*, e1000361.

Gregorian, C., Nakashima, J., Le Belle, J., Ohab, J., Kim, R., Liu, A., Smith, K.B., Groszer, M., Garcia, A.D., Sofroniew, M.V., Carmichael, S.T., Kornblum, H.I., Liu, X., and Wu, H. (2009). Pten deletion in adult neural stem/progenitor cells enhances constitutive neurogenesis. J. Neurosci. *29*, 1874–1886.

Hadjilambreva, G., Mix, E., Rolfs, A., Müller, J., and Strauss, U. (2005). Neuromodulation by a cytokine: interferon-beta differentially augments neocortical neuronal activity and excitability. J. Neurophysiol. *93*, 843–852.

Hosseini, S., Wilk, E., Michaelsen-Preusse, K., Gerhauser, I., Baumgärtner, W., Geffers, R., Schughart, K., and Korte, M. (2018). Long-term neuroinflammation induced by influenza A virus infection and the impact on hippocampal neuron morphology and function. J. Neurosci. *38*, 3060–3080.

Hwang, S.Y., Hertzog, P.J., Holland, K.A., Sumarsono, S.H., Tymms, M.J., Hamilton, J.A., Whitty, G., Bertoncello, I., and Kola, I. (1995). A null mutation in the gene encoding a type I interferon receptor component eliminates antiproliferative and antiviral responses to interferons alpha and beta and alters macrophage responses. Proc. Natl. Acad. Sci. USA *92*, 11284–11288.

Ignatowski, T.A., and Spengler, R.N. (2008). Cytokines in synaptic function. NeuroImmune Biol. *6*, 109–143.

Kaech, S., and Banker, G. (2006). Culturing hippocampal neurons. Nat. Protoc. *1*, 2406–2415.

Kamphuis, E., Junt, T., Waibler, Z., Forster, R., and Kalinke, U. (2006). Type I interferons directly regulate lymphocyte recirculation and cause transient blood lymphopenia. Blood *108*, 3253–3261.

Korte, M., and Schmitz, D. (2016). Cellular and System Biology of Memory: Timing, Molecules, and Beyond. Physiol. Rev. *96*, 647–693.

Lee, H.-C., Tan, K.-L., Cheah, P.-S., and Ling, K.-H. (2016). Potential role of JAK-STAT signaling pathway in the neurogenic-to-gliogenic shift in down syndrome brain. Neural Plast. *2016*, 7434191.

McAfoose, J., and Baune, B.T. (2009). Evidence for a cytokine model of cognitive function. Neurosci. Biobehav. Rev. *33*, 355–366.

McGlasson, S., and Hunt, D. (2017). Neuroinflammation: Synapses pruned in lupus. Nature *546*, 482–483.

Mehler, M.F., and Kessler, J.A. (1998). Cytokines in Brain Development and Function. In Advances in Protein Chemistry, F.M. Richards, D.S. Eisenberg, and P.S. Kim, eds. (Academic Press), pp. 223–251.

Mendoza-Fernández, V., Andrew, R.D., and Barajas-López, C. (2000). Interferon-α inhibits long-term potentiation and unmasks a long-term depression in the rat hippocampus. Brain Res. *885*, 14–24.

Morris, R. (1984). Developments of a water-maze procedure for studying spatial learning in the rat. J. Neurosci. Methods *11*, 47–60.

Moser, M.-B., Trommald, M., and Andersen, P. (1994). An increase in dendritic spine density on hippocampal CA1 pyramidal cells following spatial learning in adult rats suggests the formation of new synapses. Proc. Natl. Acad. Sci. USA *91*, 12673–12675.

Müller, U., Steinhoff, U., Reis, L.F., Hemmi, S., Pavlovic, J., Zinkernagel, R.M., and Aguet, M. (1994). Functional role of type I and type II interferons in antiviral defense. Science *264*, 1918–1921.

Murray, P.J. (2007). The JAK-STAT signaling pathway: input and output integration. J. Immunol. *178*, 2623–2629.

Ota, Y., Zanetti, A.T., and Hallock, R.M. (2013). The role of astrocytes in the regulation of synaptic plasticity and memory formation. Neural Plast. *2013*, 185463.

Owens, T., Khorooshi, R., Wlodarczyk, A., and Asgari, N. (2014). Interferons in the central nervous system: a few instruments play many tunes. Glia *62*, 339–355.

Papageorgiou, I.E., Fetani, A.F., Lewen, A., Heinemann, U., and Kann, O. (2015). Widespread activation of microglial cells in the hippocampus of chronic

epileptic rats correlates only partially with neurodegeneration. Brain Struct. Funct. *220*, 2423–2439.

Plioplys, A.V. (1988). Expression of the 210 kDa neurofilament subunit in cultured central nervous system from normal and trisomy 16 mice: regulation by interferon. J. Neurol. Sci. *85*, 209–222.

Prieto-Gomez, B., Reyes-Vazquez, C., and Dafny, N. (1983). Differential effects of interferon on ventromedial hypothalamus and dorsal hippocampus. J. Neurosci. Res. *10*, 273–278.

Riazi, K., Galic, M.A., Kentner, A.C., Reid, A.Y., Sharkey, K.A., and Pittman, Q.J. (2015). Microglia-dependent alteration of glutamatergic synaptic transmission and plasticity in the hippocampus during peripheral inflammation. J. Neurosci. *35*, 4942–4952.

Santello, M., Bezzi, P., and Volterra, A. (2011). TNFα controls glutamatergic gliotransmission in the hippocampal dentate gyrus. Neuron *69*, 988–1001.

Schneider, H., Pitossi, F., Balschun, D., Wagner, A., del Rey, A., and Besedovsky, H.O. (1998). A neuromodulatory role of interleukin-1beta in the hippocampus. Proc. Natl. Acad. Sci. USA *95*, 7778–7783.

Stellwagen, D., and Malenka, R.C. (2006). Synaptic scaling mediated by glial TNF-alpha. Nature *440*, 1054–1059.

Swanson, R.A. (2005). Astrocyte neurotransmitter uptake, H. Neuroglia, Kettenmann., and B.R. Ransom, eds. (Oxford University Press), pp. 346–354.

Thaney, V.E., O'Neill, A.M., Hoefer, M.M., Maung, R., Sanchez, A.B., and Kaul, M. (2017). IFNβ Protects Neurons from Damage in a Murine Model of HIV-1 Associated Brain Injury. Sci. Rep. *7*, 46514.

Theodosis, D.T., Poulain, D.A., and Oliet, S.H.R. (2008). Activity-dependent structural and functional plasticity of astrocyte-neuron interactions. Physiol. Rev. *88*, 983–1008.

Tovey, M.G., Streuli, M., Gresser, I., Gugenheim, J., Blanchard, B., Guymarho, J., Vignaux, F., and Gigou, M. (1987). Interferon messenger RNA is produced constitutively in the organs of normal individuals. Proc. Natl. Acad. Sci. USA *84*, 5038–5042.

Tronche, F., Kellendonk, C., Kretz, O., Gass, P., Anlag, K., Orban, P.C., Bock, R., Klein, R., and Schütz, G. (1999). Disruption of the glucocorticoid receptor gene in the nervous system results in reduced anxiety. Nat. Genet. *23*, 99–103.

Vikman, K., Robertson, B., Grant, G., Liljeborg, A., and Kristensson, K. (1998). Interferon-γ receptors are expressed at synapses in the rat superficial dorsal horn and lateral spinal nucleus. J. Neurocytol. *27*, 749–759.

Vikman, K.S., Owe-Larsson, B., Brask, J., Kristensson, K.S., and Hill, R.H. (2001). Interferon-γ-induced changes in synaptic activity and AMPA receptor clustering in hippocampal cultures. Brain Res. *896*, 18–29.

Vorhees, C.V., and Williams, M.T. (2006). Morris water maze: procedures for assessing spatial and related forms of learning and memory. Nat. Protoc. *1*, 848–858.

Walsh, R.N., and Cummins, R.A. (1976). The Open-Field Test: a critical review. Psychol. Bull. *83*, 482–504.

Wei, J., Ma, Y., Wang, L., Chi, X., Yan, R., Wang, S., Li, X., Chen, X., Shao, W., and Chen, J.L. (2017). Alpha/beta interferon receptor deficiency in mice significantly enhances susceptibility of the animals to pseudorabies virus infection. Vet. Microbiol. *203*, 234–244.

Whishaw, I.Q. (2004). Posterior neocortical (visual cortex) lesions in the rat impair matching-to-place navigation in a swimming pool: a reevaluation of cortical contributions to spatial behavior using a new assessment of spatial versus nonspatial behavior. Behav. Brain Res. *155*, 109–116.

Wilson, C.J., Finch, C.E., and Cohen, H.J. (2002). Cytokines and cognition–the case for a head-to-toe inflammatory paradigm. J. Am. Geriatr. Soc. *50*, 2041–2056.

Wolf, S.A., Boddeke, H., and Kettenmann, H. (2017). Microglia in physiology and disease. Annu. Rev. Physiol *79*, 619–643.

Zhu, Y., Romero, M.I., Ghosh, P., Ye, Z., Charnay, P., Rushing, E.J., Marth, J.D., and Parada, L.F. (2001). Ablation of NF1 function in neurons induces abnormal development of cerebral cortex and reactive gliosis in the brain. Genes Dev. *15*, 859–876.

Ziv, Y., Ron, N., Butovsky, O., Landa, G., Sudai, E., Greenberg, N., Cohen, H., Kipnis, J., and Schwartz, M. (2006). Immune cells contribute to the maintenance of neurogenesis and spatial learning abilities in adulthood. Nat. Neurosci. *9*, 268–275.

STAR★METHODS

KEY RESOURCES TABLE

REAGENT or RESOURCE	SOURCE	IDENTIFIER
Antibodies		
Anti-GAPDH antibody produced in rabbit	Sigma-Aldrich	Cat# G9545; RRID:AB_796208
Anti-GFAP, mouse monoclonal	Sigma-Aldrich	Cat#G3893; RRID:AB_477010
Anti-IBA1 (Polyclonal rabbit purified antibody)	Synaptic Systems	Cat# 234 003; RRID:AB_10641962
Anti-Rabbit IgG (whole molecule)–Peroxidase antibody produced in goat	Sigma-Aldrich	Cat# A0545; RRID:AB_257896
Cy2 AffiniPure Goat Anti-Rabbit IgG (H+L)	Jackson ImmunoResearch Laboratories	Cat# 111-225-144; RRID:AB_2338021
Cy3 AffiniPure Goat Anti-Mouse IgG + IgM (H+L)	Jackson ImmunoResearch Laboratories	Cat#115-165-068; RRID:AB_2338686
Cy3 AffiniPure Goat Anti-Rabbit IgG (H+L)	Jackson ImmunoResearch Laboratories	Cat#111-165-144; RRID:AB_2338006
EAAT1/GLAST-1/SLC1A3 antibody	Novus Biologicals	Cat# NB100-1869; RRID:AB_2190597
IFNAR1 Monoclonal Antibody (MAR1-5A3)	Thermo Fisher Scientific	Cat# 16-5945-85; RRID:AB_1210688
Mouse IgG1 kappa Isotype Control (P3.6.2.8.1)	Thermo Fisher Scientific	Cat# 14-4714-82; RRID:AB_470111
Chemicals, Peptides, and Recombinant Proteins		
BenchStable DMEM	Thermo Fisher Scientific	Cat# A4192101
Bovine Serum Albumin	Sigma-Aldrich	Cat# A7906
$CaCl_2$	Applichem	Lot: 4U010421
CNQX disodium salt	Tocris	Cat# 1045
cOmplete Protease Inhibitor Cocktail	Sigma-Aldrich	Cat# 04693116001
D-AP5 (APV)	Tocris	Cat# 0106
DAPI	Sigma-Aldrich	Cat# D9542
D-glucose	Roth	Art.-Nr. HN06.3
Dimethyl sulfoxide (DMSO)	Sigma-Aldrich	Cat# 472301
Fluoro-Gel mounting medium	Electron Microscopy Sciences	Cat# 17985-10
GBSS	Sigma-Aldrich	G9779-500ML
GIBCO® goat serum	Thermo Fisher Scientific	Cat# 16210072
GIBCO B-27 Supplement	Fisher Scientific	Cat# 11530536
GIBCO CTS Neurobasal Medium	Fisher Scientific	Cat# 12043479
GIBCO Fetal Bovine Serum	Fisher Scientific	Cat# 11573397
GIBCO HBSS 10X	Fisher Scientific	Cat# 14065049
GIBCO L-Glutamine	Fisher Scientific	Cat# 15410314
GIBCO N-2 Supplemen	Fisher Scientific	Cat# 15410294
Glycine	Applichem	Cat# A1067
KCl	Applichem	Lot: 0000574737
KH_2PO_4	Applichem	Lot: 4Q016683
Lipofectamine® 2000	Invitrogen	REF. 11668-019
Luminata™ (Immobilon Crescendo Western HRP substrate	Merck Millipore	Cat# WBLUR0100
$MgSO_4$	Applichem	Lot: 3E000057
NaCl	Applichem	Lot: 8Q012497
$NaHCO_3$	Roth	Art.-Nr. HN01.1

(*Continued on next page*)

Continued

REAGENT or RESOURCE	SOURCE	IDENTIFIER
Permount Mounting Medium	Fisher Scientific	Cat# SP15-100
PhosSTOP	Sigma-Aldrich	Cat# 04 906 837 001
Poly-L-lysine solution	Sigma-Aldrich	CAS# 25988-63-0
Recombinant Mouse IFN-beta Protein, CF	R&D Systems	Cat# 8234-MB-010/CF
Strychnine	Sigma-Aldrich	CAS Nr. 57-24-9
TFB-TBOA	Tocris	Cat# 2532
Triton® X-100 Molecular Biology grade BC	Applichem	Cat# A4975
Trypsin-EDTA Solution 10X	Sigma-Aldrich	CAS# 9002-07-7
TWEEN® 20	Sigma-Aldrich	Cat# P9416
Critical Commercial Assays		
FD Rapid GolgiStain Kit	FD NeuroTechnologies, Inc.	Cat# PK401
Experimental Models: Organisms/Strains		
C57BL/6J OlaHsd mice	Harlan-Winkelmann or Janvier	Cat# 057 (H-W)
GFAP-Cre $^{+/-}$ mice	NCI Mouse Repository	Cat# 01XN3
IFNAR $^{-/-}$ mice	Kamphuis et al., 2006	N/A
IFNAR $^{fl/fl}$ mice	Kamphuis et al., 2006	N/A
IFN-β $^{-/-}$ mice	Erlandsson et al.,1998	N/A
Nes-Cre $^{+/-}$ mice	The Jackson Laboratory	Cat# 003771
Syn1-Cre $^{+/-}$ mice	The Jackson Laboratory	Cat# 003966
Recombinant DNA		
pAcGFP1-F Vector	Clontech	Cat# 632511
Software and Algorithms		
ANY-maze	Stoelting	RRID:SCR_014289 https://www.stoeltingco.com/
EasyWin32	Herolab	https://www.herolab.de/index.php/de/gel-dokumentation/analyse-software.html
Fiji	BioVoxxel	RRID:SCR_015825 http://www.biovoxxel.de/
IntraCell Version 1.5	(C) 2000 Institute for Neurobiology Magdeburg	N/A
Prism 7	GraphPad	https://www.graphpad.com/scientific-software/prism/
Video Mot 2	TSE Systems	https://www.tse-systems.com
G*Power Version 3.1.9.4	Heinrich Heine University Düsseldorf, Germany	http://www.psychologie.hhu.de/arbeitsgruppen/allgemeine-psychologie-und-arbeitspsychologie/gpower.html

RESOURCE AVAILABILITY

Lead Contact

Further information and requests for resources and reagents should be directed to and will be fulfilled by the Lead Contact, Martin Korte (m.korte@tu-bs.de).

Materials Availability

This study did not generate new unique reagents.

Data and Code Availability

This study did not generate/analyze [datasets/code].

EXPERIMENTAL MODEL AND SUBJECT DETAILS

Mice

In this study male and female C57BL/6J OlaHsd mice, also referred to as wild-type (*WT*), were originally purchased from Harlan-Winkelmann, Germany, or Janvier, France and bred under standard housing conditions.

Inactivation of the IFNAR1 gene in embryonic stem cells was achieved by homologous recombination (Müller et al., 1994). The findings of Müller and colleagues defined that, mice lacking the IFNAR1 subunit of the IFN receptor (conventional knockout) were completely unresponsive to all type I IFN, including IFN-α and IFN-β. This suggests that the existence of IFNAR1 polypeptide chain is likewise essential for IFN to mediate signal transduction. IFNAR1-deficient mice (*Ifnar*$^{-/-}$) did not show any overt anomalies, however, they were unable to cope with viral infections efficiently despite otherwise normal immune responses (Müller et al., 1994; Wei et al., 2017). *Ifnar*$^{-/-}$ animals were extensively backcrossed (more than 10 generation) with C57BL/6J OlaHsd mice to ensure a homogeneous genetic background. *Ifnar*$^{-/-}$ mice were bred with Wt animals and then hemizygous animals were used to generate *Ifnar*$^{-/-}$ mice to control the genetic drift in the colony.

In order to enable selective depletion of IFNAR on different CNS cell types, conditional IFNAR mice (*Ifnar*$^{fl/fl}$) (Kamphuis et al., 2006) were intercrossed with transgenic mice that express Cre recombinase in neuroectodermal cells including neurons, astrocytes and oligodendrocytes (Nestin-Cre, Cre transgene starting from embryonic day 12.5, E12.5, NesCre$^{+/-}$IFNAR$^{fl/fl}$) (Tronche et al., 1999), neurons (Synapsin I-Cre (E12.5), Syn1Cre$^{+/-}$IFNAR$^{fl/fl}$) (Zhu et al., 2001) or astrocytes (E14.5, GFAPCre$^{+/-}$IFNAR$^{fl/fl}$) (Bajenaru et al., 2002), respectively, and backcrossed into the C57BL/6J OlaHsd background. The astrocyte specificity of GFAPCre$^{+/-}$IFNAR$^{fl/fl}$ mice has already been described previously (Chhatbar et al., 2018). In this line Cre recombinase activity in a subpopulation of adult neural stem cells in the subventricular zone was distinguished before, however, GFAP-Cre mice are reported to have no Cre recombinase activity in postnatal or adult neural stem cells or their progeny from the hippocampus or other brain regions (Gregorian et al., 2009). Thus, GFAP-Cre mice are particularly useful for selective targeting of astrocytes (Bajenaru et al., 2002; Chhatbar et al., 2018).

Ifnb$^{-/-}$ mice (Erlandsson et al., 1998) were backcrossed into the C57BL/6J OlaHsd background in the same way as *Ifnar*$^{-/-}$ mice.

All mice were bred and kept under specific-pathogen-free conditions in the central mouse facility of the Twincore, Centre for Experimental and Clinical Infection Research, Hannover, and at the Helmholtz Centre for Infection Research, Braunschweig. In this study, both male and female mice were used.

The experiments performed with mice were approved according to the animal welfare law in Germany. All protocols used in this project have been reviewed and approved by the local committees at TU Braunschweig and the authorities (LAVES, Oldenburg, Germany - 33.19-42502-04-18/2995) according to the national guidelines of the animal welfare law in Germany ('Tierschutzgesetz in der Fassung der Bekanntmachung vom 18. Mai 2006 (BGBl. I S. 1206, 1313), das zuletzt durch Artikel 20 des Gesetzes vom 9. Dezember 2010 (BGBl. I S. 1934) geändert worden ist.').

Primary embryonic hippocampal culture

For different pharmacological approaches, primary embryonic hippocampal cultures were prepared as previously described (Kaech and Banker, 2006). Briefly, pregnant female *WT* or *Ifnar*$^{-/-}$ mice were rapidly killed by cervical dislocation for harvesting hippocampi at embryonic day E18.5. Next, the uterus was opened and the embryos were collected and decapitated immediately. The heads of the embryos were immersed in ice-cold Gey's balanced salt solution (GBSS, Sigma-Aldrich). Subsequently, brains of embryos were isolated, hippocampi were dissected and immersed in ice-cold GBSS. Hippocampi were transferred into a tube containing 1 mL of trypsin-EDTA solution (Sigma-Aldrich) and incubated for 30 min at 37°C. After the incubation time, trypsin solution was removed and hippocampi were washed six times with 1 mL of DMEM medium (Thermo Fisher Scientific) containing 2% fetal goat serum (Thermo Fischer Scientific). Afterward, hippocampi were homogenized and dissociated by trituration using a glass pipette and centrifuged for 5 min at 1500 rpm. The supernatant was removed and the cell sediment was resolved in 1 mL of Neurobasal medium (GIBCO) containing glutamine (200 mM), 1% N2 and 2% B-27 (GIBCO) supplements referred as complete medium. 7×10^4 cells in 150 µL of complete medium were plated on poly-L-lysine (Sigma-Aldrich) coated coverslip (15 mm diameter). The cells were cultured in 24 well plates and incubated for 3 h at 37°C. Finally, 350 µL of pre-warmed complete medium was added to each well and plates were kept in an incubator at 37°C for 21 days. Once a week, 100 µL of culture medium per well were replaced by fresh complete medium.

Acute mouse hippocampal slices

Acute hippocampal slices were prepared from 6-8 weeks old conventional and conditional knockout and respective control mice. Briefly, mice were deeply anesthetized with 100% CO_2 then sacrificed and brains were quickly removed. Right hemispheres were immersed into ice-cold carbogenated (95% O_2 and 5% CO_2) artificial cerebrospinal fluid (ACSF) and the left hemispheres were transferred into the Golgi-Cox staining solution for further morphological analysis. ACSF contained 124 mM NaCl, 4.9 mM KCl, 1.2 mM KH_2PO_4, 2.0 mM $MgSO_4$, 2.0 mM $CaCl_2$, 24.6 mM $NaHCO_3$ and 10 mM D-glucose at pH = 7.4. Afterward, the hippocampus was dissected and transverse hippocampal slices (400 µm) were obtained by using a manual tissue chopper. The hippocampal slices were transferred to an interface recording chamber (Scientific System Design), where they were incubated at 32°C with a constant flow rate (0.5 ml/min) of carbogenated ACSF for 2 hours prior to the start of recordings.

METHOD DETAILS

Behavioral assays

For behavioral evaluation, 8-10 weeks old conventional or conditional IFNAR as well as IFN-β knockout mice and respective control animals were assigned to different groups. All behavioral experiments were performed at the same time of day during the light period between 9:00 to 16:00 by an experimenter blind to all groups.

Open field test

In this study, spontaneous locomotor activity and explorative behavior of mice were assessed using the open field test as previously described (Walsh and Cummins, 1976). Briefly, mice were allowed to freely explore the open field apparatus (40cm × 40cm × 40cm) for 5 min. The central area of the arena was specified as the center part (30cm × 30cm). Between animals, the apparatus was completely cleaned with Bacillol® to reduce odor cues. Movement data including total distance traveled, average speed and percentage of activity in the periphery and center parts of the arena were collected by Video Mot 2 (TSE Systems GmbH, Bad Homburg, Germany) or ANY-maze (Stoelting, USA) behavioral tracking software.

Morris water maze test

In order to investigate cognitive behavior in mice, spatial learning and memory formation was assessed using the Morris water maze paradigm. Spatial learning in the Morris water maze is a hippocampus-dependent task where the animals have to locate a hidden platform using visual cues surrounding the pool (Morris, 1984; Vorhees and Williams, 2006). The maze was comprised of a circular pool 160 cm in diameter which was filled with water at 19-20 C colored opaque (Titaandioxide, Euro OTC Pharma). The transparent platform was 10 cm in diameter and hidden 1 cm underneath the surface of the water. Prior to the training, a visible platform task was performed as a pre-training and used to ensure that swimming ability and visual acuity were intact in all experimental groups, moreover, this phase was important for the animals to get accustomed to the test situation. During this phase, the animals had two trials (maximum of 60 s each) per day for three consecutive days to reach the visible platform, the position was alternated during the trials (Data are not shown). Subsequently, training in the Morris water maze was performed for 8 days with the invisible platform located in the northwest (NW) quadrant. Each day, animals were placed in the water for four trials, with different starting points (SW, S, E, and NE) randomly at a 5 min intertrial interval. The animals were permitted to swim freely for 60 s or until the platform was reached. Otherwise, they were guided to the platform and allowed to sit on it for 20 s.

For qualitative aspects of spatial learning and memory formation during 8 days of acquisition training, the pathway map to find the platform was analyzed to evaluate different searching strategies. For this purpose, the relative presence in different zones of the swimming pool including a doughnut-shaped annulus zone (Ring with a diameter of 20 cm at the same distance from the wall as the platform), the center area (Circular region covering the center until 25 cm distance from the walls, including the platform) and Wishaw's corridors (Corridor from the respective starting position leading to the platform with a width of 12 cm) were assessed (Hosseini et al., 2018). Over time, mice switch from egocentric hippocampus-independent strategies including scanning characterized by > 75% presence in the center area, chaining characterized by > 75% presence in the doughnut-shaped annulus zone and random search characterized by > 80% coverage of the surface to an allocentric direct swimming strategy characterized by > 50% presence in the Wishaw's corridors (goal corridor) which depends highly on the hippocampus (Figure S2A) (Garthe et al., 2009; Garthe and Kempermann, 2013; Whishaw, 2004).

For evaluation of reference memory, three probe trial tests were performed at the third and at the sixth day of the acquisition training, prior to the training session on that day. Another reference memory test was performed 24 h after the last day of acquisition training (day 9). During the probe trial, the platform was removed and the animals were allowed to swim freely for 45 s.

All data including swimming time (latency to reach the platform), percentage of time spent in the four quadrants of the pool, percentage of time spent in the border (thigmotaxis), annulus (chaining), central circle (scanning) zones and Whishaw's corridors (direct swimming) of the pool were collected by Video Mot 2 (TSE Systems GmbH, Bad Homburg, Germany) or ANY-maze (Stoelting, USA) behavioral tracking software.

Electrophysiological experiments

Field excitatory postsynaptic potentials (fEPSPs) were recorded in the stratum radiatum of the CA1 region in acute hippocampal slices. Responses were evoked by electrical stimulation of the Schaffer collateral pathway using two monopolar, lacquer coated stainless-steel electrodes (5 MΩ; AM Systems). These stimulation electrodes (S1 and S2) were positioned equidistantly on both sides of the recording electrode and by this means two independent stimulation pathways could be used for the same CA1 recording region. For recording fEPSPs (measured as the first slope function), the recording electrode (5 MΩ; AM Systems) was placed in the CA1 apical dendritic layer (at least 20 μm away from the stratum pyramidale) and signals were amplified by a differential amplifier (Model 1700, AM Systems). The signals were digitized using a CED 1401 analog-to-digital converter (Cambridge Electronic Design). An input-output curve (afferent stimulation versus fEPSP slope) for assessment of basal synaptic transmission was generated after the pre-incubation period. Test stimulation intensity was modified to be adjusted to extract fEPSP slope as 40% of the maximal fEPSP response for both synaptic inputs S1 and S2. To investigate short-term plasticity, a paired-pulse stimulation protocol was used with two consecutive stimuli with equal intensity from one of the stimulating electrodes in each hippocampal slice. Paired-pulse facilitation (PPF) was extracted from the fEPSP slopes as a response to the second stimulation over the first one at different interpulse intervals of 10, 20, 40, 60, 80, and 100 ms. To investigate long-term potentiation, 20 min after baseline recording LTP was induced by

Theta-burst stimulation (TBS) including four bursts at 100 Hz repeated 10 times in a 200 ms interval. This stimulation was repeated three times in a 10 s interval. Only healthy sections with a stable baseline were included in the electrophysiological data analysis. The slope of fEPSPs was measured over time and normalized to the baseline. Data acquisition and offline analysis were performed using IntraCell software (Version 1.5, LIN, Magdeburg, 2000).

IFNAR1 antibody treatment in electrophysiological recording

To investigate the acute effect of blocking IFN signaling on CA1 hippocampal neurons, blocking antibody treatment during the electrophysiological recording was performed. For this purpose, acute hippocampal slices obtained from 6-8 weeks old Wt mice were pretreated for 1 h before the recording with IFNAR1 monoclonal antibody (MAR1-5A3, Functional Grade, eBioscience, Thermo Fisher Scientific) or mouse IgG1 kappa isotype control antibody (P3.6.2.8.1, Thermo Fisher Scientific) dissolved at the final concentration of 10 μg/ml in ACSF.

Golgi-Cox staining

To investigate the effect of IFN signaling deficiency on hippocampal neuron morphology, Golgi-Cox staining was performed. For this purpose, the left hemispheres of 6-8 weeks old conventional and conditional knockout and respective control mice were incubated in FD rapid Golgi stain kit (FD NeuroTechnologies, Inc., Columbia, USA) according to the manufacturer's protocol. Afterward, hemispheres were blocked in 2% agar and 200 μm thick coronal sections were cut with a vibratome (Leica VT 1000 S) and mounted on gelatin-coated glass slides. Subsequently, the sections were processed for signal development before being dehydrated through graded alcohols and mounted using Permount (Fisher Scientific).

Transfection

Three weeks old primary embryonic hippocampal cultures (day *in vitro* (DIV) 21) were transfected using Plasmid DNA pAcGFP1-F (farnesylated enhanced green fluorescent protein, CMV promoter, Clontech) to visualize the neurons and allow for further morphological analysis. For transfection, 1 μg of DNA and 2 μL of Lipofectamine®2000 (Invitrogen) per well were mixed separately in 50 μL pre-warmed Neurobasal medium and incubated at room temperature for 5 min. Afterward, both solutions were combined and incubated for 20 min at room temperature. After the incubation time, the old complete culture medium was collected from each well and 300 μL of fresh pre-warmed Neurobasal medium without any further supplements was added to each well. Subsequently, 100 μL of transfection solution was added dropwise to each well. Plates were incubated for 50 min at 37°C in the incubator. Next, the transfection medium was replaced with old collected complete culture medium and plates were incubated for another 48 hours at 37°C in the incubator before the respective experiment started.

Chemical LTP (cLTP) induction in primary embryonic hippocampal culture

To investigate structural synaptic plasticity, NMDA receptor dependent LTP was induced chemically (cLTP) by glycine. For this purpose, transfected cultures were incubated in 500 μL of Hank's balanced salt solution (HBSS 1X, GIBCO) for 10 min at room temperature followed by another 10 min incubation in HBSS 1X without magnesium containing 200 μM glycine (AppliChem) and 3 μM Strychnine (blocker for inhibitory ionotropic glycine receptor) (Sigma-Aldrich) (Fortin et al., 2010). Afterward, the solution was removed and 500 μL of HBSS 1X per well were added and cells were incubated for another 50 min at room temperature before fixation. Control wells were treated only with HBSS 1X. Finally, cells were fixed using 4% paraformaldehyde (PFA) for 15 min at room temperature. The cultures were washed three times (each time 5 min) with PBS 1X. After washing, the coverslips were mounted using Fluoro-gel mounting medium (Electron Microscopy Sciences, Hatfield, PA).

Pharmacological treatments

Primary embryonic hippocampal cultures obtained from Wt or *Ifnar*$^{-/-}$ animals were treated with IFN-β (1000 U/ml, R&D Systems) alone for 10 min or accompanied by glycine and strychnine in HBSS 1X without magnesium for cLTP induction at room temperature. Then, the cells were incubated in HBSS 1X for another 50 min before fixation. To acutely block IFNAR signaling primary embryonic hippocampal cultures were treated with mouse IFNAR1 monoclonal antibody (10 μg/ml) (MAR1-5A3, Thermo Fisher Scientific) or mouse IgG1 kappa isotype control antibody (10 μg/ml) (P3.6.2.8.1, Thermo Fisher Scientific) for 10 min alone or accompanied with glycine and strychnine in HBSS 1X without magnesium for cLTP induction at room temperature.

To investigate whether IFN-β action depends on ionotropic glutamate receptor signaling primary embryonic hippocampal cultures were treated with 1000 U/ml IFN-β accompanied by NMDA receptor antagonist, APV (50 μM, (2R)-amino-5-phosphonovaleric acid, Tocris) and a competitive AMPA receptor antagonist, CNQX (20 μM, 6-cyano-7-nitroquinoxaline-2,3-dione, Tocris) in HBSS 1X without magnesium for 10 min. Afterward, the cells were incubated for another 50 min in HBSS 1X at room temperature before fixation.

To investigate the effects of a glial glutamate transporter inhibitor (as an emulator of IFN) on structural synaptic plasticity, primary embryonic hippocampal cultures were treated with 20 nM TFB-TBOA alone for 10 min or accompanied by glycine and strychnine in HBSS 1X without magnesium for cLTP induction. Afterward, the cells were incubated for another 50 min in HBSS 1X at room temperature before fixation. TFB-TBOA ((2S, 3S)-3-[3-[4-(trifluoromethyl)benzoylamino]benzyloxy]aspartate, Tocris) is a potent and selective glial glutamate transporter EAAT1 and EAAT2 inhibitor, nevertheless it has no effect on EAAT4 and EAAT5 or a wide range of neuronal glutamate receptors and transports (Bozzo and Chatton, 2010). TFB-TBOA was solved in DMSO and the final concentration of DMSO was less than 0.5% in solution. An equal amount of DMSO was added to control and cLTP induced cells.

Immunohistochemistry

To determine the inflammatory responses and GLAST expression in the hippocampus of mice lacking IFNAR, brains of 6-8 weeks old conventional and conditional IFNAR knockout and respective control mice were isolated and fixed in 4% paraformaldehyde (PFA) for 24 hours and then cryoprotected in 30% sucrose solution in 0.1 M phosphate buffer (PB) for 24 hours and stored in Tissue-Tek® O.C.T. compound (A.Hartenstein Laborversand) at −70°C. For fluorescence immunostaining, 30 μm sections were cut using a freezing microtome (Frigomobil, R.Jung Heidelberg, Germany). Afterward, five successive sections were washed with PBS 1X and blocked in PBS 1X solution containing 0.2% Triton X-100, 10% goat serum and 1% BSA for 1 hour at room temperature. Sections were incubated overnight at 4°C with ionized calcium-binding adaptor molecule 1 (IBA-1) (1:1000; rabbit polyclonal, Synaptic System) or EAAT1/GLAST-1/SLC1A3 (Glutamate aspartate transporter) (1:1000; rabbit polyclonal, Novus Biologicals) primary antibodies diluted in PBS 1X, 0.2% Triton X-100 and 10% goat serum. The secondary antibody was Cy™3-conjugated AffiPure Goat Anti-Rabbit IgG (H+L) (1:500; Jackson ImmunoResearch, USA) which was diluted in PBS 1X. Sections were washed by PBS 1X thoroughly (30 min) twice and stained with 4′,6-diamidino-2-phenylindole (DAPI) (Sigma-Aldrich) subsequently followed by mounting with Fluoro-gel medium (Electron Microscopy Sciences, Hatfield, PA).

Immunocytochemistry

PFA-fixed cells (on glass coverslips) were washed three times (each 5 min) with PBS 1X and were incubated 1 hour at room temperature with 0.2% Triton X-100 and 1.5% goat serum. The coverslips were washed with PBS 1X three times (each 5 min). After washing, cells were incubated in a mixture of anti-glial fibrillary acidic protein (GFAP) (1:1000; mouse monoclonal, Sigma–Aldrich) and EAAT1/GLAST-1/SLC1A3 (1:500; rabbit polyclonal, Novus Biologicals) primary antibodies diluted in 0.2% Triton X-100 and 1.5% goat serum overnight at 4°C. Then, the coverslips were washed thoroughly with PBS 1X for 30 min (3 times) and incubated in Cy™2-conjugated AffiPure Goat Anti-Rabbit IgG (H+L) (1:500; Jackson ImmunoResearch, USA) and Cy™3-conjugated AffiPure Goat Anti-Mouse IgG (H+L) (1:500; Jackson ImmunoResearch, USA) secondary antibodies diluted in PBS 1X for 1 hour at room temperature. After washing three times with PBS 1X (each 10 min), the coverslips were mounted using Fluoro-gel mounting medium (Electron Microscopy Sciences, Hatfield, PA).

Imaging and image analysis

To survey the hippocampal neuron morphology in Golgi-Cox stained slices, second- or third-order branches of apical and basal dendrites within the CA1 subregion of the hippocampus (10 cells per animal) were imaged in three-dimensions (z stack thickness of 0.5 μm) using an Axioplan 2 imaging microscope (Zeiss) equipped with a 63X (N.A. 1) oil objective and a digital camera (AxioCam MRm, Zeiss). In all selected neurons, spine density per micrometer dendrite was calculated using Fiji software (BioVoxxel) on the segments of dendritic branches with a length of more than 60-70 μm which were located at least 50 μm away from the soma. The total number of spines along the segments of dendritic branches was counted manually by an investigator blinded to all experimental groups.

In primary embryonic hippocampal cultures, only neurons (5 cells per coverslips) without any signs of degeneration or physical damage were chosen. Images of apical dendrites of neurons were taken and spine density was calculated as described above. In addition, for further morphological assessment, 20 spines were randomly selected along each dendrite and the spine head diameter was measured using Fiji software (BioVoxxel) by an investigator blinded to all experimental groups.

Images from the anti-IBA-1 staining in the CA1 region were taken in three-dimensions (z stack thickness of 1 μm) using an Axioplan 2 imaging microscope (Zeiss) microscope equipped with an ApoTome module (Zeiss), a 20X objective (N.A. 0.8) and a digital camera (AxioCam MRm, Zeiss). To quantify the density of microglia, a region of interest (ROI) was drawn in each frame of the hippocampal CA1 subregion and the total number of IBA-1 positive cells with clearly visible nuclei were counted manually by Fiji software (BioVoxxel) and the sampled volume was calculated. Results are expressed as the number of cells per mm^3 tissues and then normalized to control. For morphometric analysis of IBA-1 positive cells, at least 30 microglial cells (6 cells per each ROI) were randomly selected in CA1 hippocampal subregion of anti-IBA-1 stained images from each animal. The total number of primary microglial cell processes as a possible indicator of activation was counted using Fiji software (BioVoxxel).

Anti-GLAST staining was acquired as described above with the same fluorescent light exposure time (50 ms) in all tested groups. Image analysis was performed using Fiji software (BioVoxxel). Briefly, the maximum intensity projection of anti-GLAST stained images was generated. The whole frame (same size in all groups) was considered as a region of interest and mean gray value in ROIs were measured. In each frame mean gray value of three regions that had no fluorescence was assessed as background and subtracted from ROIs mean gray value to calculate the corrected total fluorescence intensity. Data were normalized to the control group. For the immunohistochemical experiments, all slides were coded and analysis was performed blindly.

The microscopic images of anti-GFAP and anti-GLAST stained primary embryonic hippocampal cultures were acquired with an Olympus Fluoview1000 Laser Scanning Microscope equipped with a UPLFLN 40 x oil (N.A. 1.3) objective and the software Olympus Fluoview Ver. 4.0a at a constant laser exposure percentage with the pixel size of 0.099 μm. Image analysis was conducted using Fiji software (BioVoxxel). Briefly, the maximum intensity projection of anti-GLAST stained images was generated. Using the polygon selection tool, the area of the cell body of a defined astrocyte (GFAP and GLAST positive cell) was measured, and then the GLAST positive area was calculated as a limited area with a threshold set 5 to 10% in all images (to subtract the background). Using the analyze particle tool, total immuno-positive areas for GLAST were measured in the cell body and the final data was expressed as the ratio of GLAST positive area/total cell body area multiple 100.

Western Immunoblotting

To quantify GLAST/excitatory amino acid transporter (EAAT1) expression as a marker of astrocytic glutamate regulation in the hippocampus of 6-8 weeks old conventional and conditional knockout and respective control mice, Western immunoblotting was used. Briefly, mice were deeply anesthetized with CO_2 and decapitated. Hippocampi were dissected and stored at −70°C. Hippocampi were homogenized in lysis buffer (TRIS-HCl 30mM pH 7,5, NaCl 150 mM, 1% Chaps) containing protease (Complete protease inhibitor cocktail tablets, Roche) and phosphatase inhibitor (PhosSTOP phosphatase inhibitor cocktail tablets, Roche). The concentration of isolated protein was measured using Bradford assay. Afterward, samples were added to 4X sodium dodecyl sulfate (SDS) sample buffer and heated to 96°C for 10 min. Equal quantities of protein samples (2 μg) were separated on 10% standard SDS gels. Then proteins were transferred to the Polyvinylidene fluoride (PVDF) membrane using a semi-dry blot. Membranes were blocked for 1 h at room temperature in Tris-buffered-saline-0.05% Tween 20 (TBS-T) and 5% non-fat dried milk and then incubated overnight at 4°C with anti-GLAST/EAAT1 (1:3000; rabbit polyclonal, Novus Biologicals) in TBS-T. After washing steps with TBS-T, membranes were incubated 1 h at room temperature with a secondary antibody (1:20000; anti-Rabbit IgG-Peroxidase antibody produced in goat, Sigma-Aldrich) in TBS-T. Anti-GAPDH (1:3000; produced in rabbit, affinity isolated antibody, Sigma-Aldrich) in TBS-T was used as a loading control for protein normalization in western blotting.

Immunoreactive bands were detected on an X-ray film by chemiluminescence using Luminata Crescendo Western HRP-Substrate (Merck Millipore). To quantify the expression of GLAST, densitometric analysis was performed using EasyWin32 software (Herolab GmbH).

QUANTIFICATION AND STATISTICAL ANALYSIS

Data were analyzed and plotted by GraphPad Prism 7 (GraphPad Software, Inc. USA) and presented as mean ± SEM. Differences in dendritic spine density, spine head diameter, immunostaining and western blotting data were subjected to a one-way ANOVA or Student's t test whereas two-way ANOVA was used for behavioral and electrophysiological experiments. Fisher's LSD and Tukey's multiple comparisons were used as a post hoc test. The minimum significance value was considered as $p < 0.05$. The minimum animal numbers in all experiments was calculated *a priori* using G*Power 3.1.9.4 software (Heinrich Heine University Düsseldorf, Germany). All statistical analysis and n of different experimental groups were reported in the respective results or figure legends.